Graduate School ETD Form 9
(Revised 12/07)

PURDUE UNIVERSITY
GRADUATE SCHOOL
Thesis/Dissertation Acceptance

This is to certify that the thesis/dissertation prepared

By Shih, Han

Entitled
STEP-GROWTH THIOL-ENE PHOTOPOLYMERIZATION TO FORM DEGRADABLE, CYTOCOMPATIBLE AND MULTI-STRUCTURAL HYDROGELS

For the degree of Master of Science in Biomedical Engineering

Is approved by the final examining committee:

Lin, Chien-Chi
Chair

Xie, Dong

Bottino, Marco

To the best of my knowledge and as understood by the student in the *Research Integrity and Copyright Disclaimer (Graduate School Form 20)*, this thesis/dissertation adheres to the provisions of Purdue University's "Policy on Integrity in Research" and the use of copyrighted material.

Approved by Major Professor(s): Lin, Chien-Chi

Approved by: Schild, John 4 / 18 / 2013
Head of the Graduate Program Date

STEP-GROWTH THIOL-ENE PHOTOPOLYMERIZATION TO FORM DEGRADABLE, CYTOCOMPATIBLE AND MULTI-STRUCTURAL HYDROGELS

A Thesis
Submitted to the Faculty
of
Purdue University
by
Han Shih

In Partial Fulfillment of the
Requirements for the Degree
of
Master of Science in Biomedical Engineering

May 2013
Purdue University
Indianapolis, Indiana

ACKNOWLEDGEMENTS

I would like to acknowledge my thesis advisor, Dr. Chien-Chi Lin, for his assistance, guidance and supervision during the entire course of this research and thesis work. Dr. Lin generously shared with me his research experience and taught me useful knowledge and skills that I am always thankful and grateful for.

I would also like to thank my advisory committee members, Dr. Dong Xie and Dr. Marco Bottino, for their time and insight for this thesis work.

In addition, I would like to thank my colleagues: Dr. Changseok Ki, Mr. Asad Raza, Ms. Yiting Hao, Mr. Andrew K. Fraser, Ms. Arika Kemp and Mr. Zach Munoz for their help and support. I thank Dr. Karl Dria, Mr. Cary Pritchard, and Mr. Yu-Hung Lin for their technical assistant. I would also like to thank Ms. Shelly Albertson for helping with documentation and Ms. Valerie Lim Diemer for assisting me in formatting this thesis. Finally, I express my gratitude to my family and friends for their support and encouragement.

TABLE OF CONTENTS

Page

Page

LIST OF TABLES

LIST OF FIGURES

Figure Page

Figure Page

Figure Page

Figure Page

Figure Page

LIST OF ABBREVIATIONS

Symbol	Description
CDGDC	5-mer peptide cysteine-aspartic acid -glycine-aspartic acid -cysteine
CGGDC	5-mer peptide cysteine-glycine-glycine-aspartic acid-cysteine
CGGGC	5-mer peptide cysteine-glycine-glycine-glycine-cysteine
CGGKC	5-mer peptide cysteine-glycine-glycine-lysine-cysteine
CGGLC	5-mer peptide cysteine-glycine-glycine-leucine-cysteine
CGGYC	5-mer peptide cysteine-glycine-glycine-tyrosine-cysteine
CRGDS	5-mer peptide cysteine-arginine-glycine-aspartic acid-serine
DTT	Dithiothresitol
EY	Eosin-Y disodium salt
hMSCs	Human mesenchymal stem cells
LAP	Lithium arylphosphinate
MIN6	Mouse insulinoma cells
NVP	1-vinyl-2 pyrrolidinone
PEG4A	Poly(ethylene glycol)-tetra-acrylate
PEG4aNB	Poly(ethylene glycol)-tetra-amide-norbornene
PEG4NB	Poly(ethylene glycol)-tetra-norbornene
PEGDA	Poly(ethylene glycol)-di-acrylate
PEGdNB	Poly(ethylene glycol)-di-norbornene
TEOA	Triethanolamine

NOMENCLATURE

Symbol	Unit	Description
E	$M^{-1}cm^{-1}$	Molar absorptivity
G'	Pa	Storage or elastic modulus
G"	Pa	Loss or viscous modulus
W_{Dry}	mg	Dried polymer weight
$W_{Swollen}$	mg	Swollen weight
k_{hyd}	day^{-1}	Apparent pseudo first-order ester hydrolysis rate constant
$\overline{M_c}$	Da	Average molecular weight between crosslinks
MW_A	Da	Molecular weight of macromer
MW_B	Da	Molecular weight of crosslinker
$\overline{v_1}$	cm^3/g	Specific volume of water
$\overline{v_2}$	cm^3/g	Specific volume of PEG
V_1	$cm^3/mole$	Molar volume of water
k'	day^{-1}	Pseudo-first order ester bond hydrolysis rate constant
$[A]_0$	M	Concentration of f_A-arm macromers in the equilibrium swelling state before the onset of network degradation
Q		Mass swelling ratio
f_A		Number of reactive functionality for macromer
f_B		Number of reactive functionality for crosslinker
v_c		Density of elastically active chains
v_2		Polymer volume fraction
χ_{12}		Flory-Huggins interaction parameter for a PEG-H_2O system
P_{Ester}		Fraction of hydrolyzed ester bonds
P_{Chain}		Fraction of intact elastic chains
N		Number of degradable units
F_{i,f_A}		Fraction of f_A-armed macromer with *i* arms still connected to the network

ABSTRACT

Shih, Han. M.S.B.M.E., Purdue University, May 2013. Step-growth Thiol-ene Photopolymerization to Form Degradable, Cytocompatible and Multi-structural Hydrogels. Major Professor: Chien-Chi Lin.

Hydrogels prepared from photopolymerization have been used for a variety of tissue engineering and controlled release applications. Polymeric biomaterials with high cytocompatibility, versatile degradation behaviors, and diverse material properties are particularly useful in studying cell fate processes. In recent years, step-growth thiol-ene photochemistry has been utilized to form cytocompatible hydrogels for tissue engineering applications. This radical-mediated gelation scheme utilizes norbornene functionalized multi-arm poly(ethylene glycol) (PEGNB) as the macromer and di-thiol containing molecules as the crosslinkers to form chemically crosslinked hydrogels. While the gelation mechanism was well-described in the literature, the network properties and degradation behaviors of these hydrogels have not been fully characterized. In addition, existing thiol-ene photopolymerizations often used type I photoinitiators in conjunction with an ultraviolet (UV) light source to initiate gelation. The use of cleavage type initiators and UV light often raises biosafety concerns. The first objective of this thesis was to understand the gelation and degradation properties of thiol-ene hydrogels. In this regard, two types of step-growth hydrogels were compared, namely thiol-ene hydrogels and Michael-type addition hydrogels. Between these two step-growth gel systems, it was found that thiol-ene click reactions formed hydrogels with higher crosslinking efficiency. However, thiol-ene hydrogels still contained significant network non-ideality, demonstrated by a high dependency of hydrogel swelling on macromer contents. In addition, the presence of ester bonds within the PEGNB macromer rendered

thiol-ene hydrogels hydrolytically degradable. Through validating model predictions with experimental results, it was found that the hydrolytic degradation of thiol-ene hydrogels was not only governed by ester bond hydrolysis, but also affected by the degree of network crosslinking. In an attempt to manipulate network crosslinking and degradation rate of thiol-ene hydrogels, different macromer contents and peptide crosslinkers with different amino acid sequences were used. A chymotrypsin-sensitive peptide was also used as part of the hydrogel crosslinkers to render thiol-ene hydrogels enzymatically degradable. The second objective of this thesis was to develop a visible light-mediated thiol-ene hydrogelation scheme using a type II photoinitiator, eosin-Y, as the only photoinitiator. This approach eliminates the incorporation of potentially cytotoxic co-initiator and co-monomer that are typically used with a type II initiator. In addition to investigating the gelation kinetics and properties of thiol-ene hydrogels formed by this new gelation scheme, it was found that the visible light-mediated thiol-ene hydrogels were highly cytocompatible for human mesenchymal stem cells (hMSCs) and pancreatic MIN6 β-cells. It was also found that eosin-Y could be repeatedly excited for preparing step-growth hydrogels with multilayer structures. This new gelation chemistry may have great utilities in controlled release of multiple sensitive growth factors and encapsulation of multiple cell types for tissue regeneration.

1. INTRODUCTION

1.1 Photopolymerization for Preparing Hydrogels

Photo-initiated radical polymerizations have received significant attention for *in situ* cell encapsulation and controlled delivery of biological molecules [1-6]. The major benefits of radical-mediated mechanism are their rapid and ambient gelation conditions, and the stability of the covalently crosslinked networks. A variety of synthetic macromers are increasingly developed for radical-mediated hydrogel synthesis via chain-growth, step-growth or mixed-mode photopolymerization [7]. In the chain-growth photopolymerization (Figure 1.1A) such as the formation of poly(ethylene glycol)-diacrylate hydrogels, radicals created by photoinitiators attack the available unsaturated carbon-carbon bond to form crosslinks. In a step-growth photopolymerization mechanism, an orthogonal reaction occurs between a proton rich species (e.g. thiol) and a π-bond at a unity stoichiometric ratio. For example, Figure 1.1B shows the formation of radicals from photoinitiators which deprotonate sulfhydryl groups to form thiyl radicals. These thiyl radicals propagate along the π-bond (e.g., norbornene or acrylate) to form chemical crosslinks. A mixed mode polymerization is the combination of both chain-growth and step-growth polymerizations. Although radical-mediated photo-gelation is well-established, its methodology has remained relatively unchanged for the past few decades. Mechanistically, a photoinitiator is required to initiate the chain-growth photopolymerization. Following light exposure, a type I or cleavage-type photoinitiator (Figure 1.2A and 1.2B) readily absorbs photons and decomposes into two primary radicals to initiate gelation [8, 9]. On the other hand, a type II photoinitiator abstracts a hydrogen from a co-initiator to generate secondary radicals and initiate crosslinking [8-11].

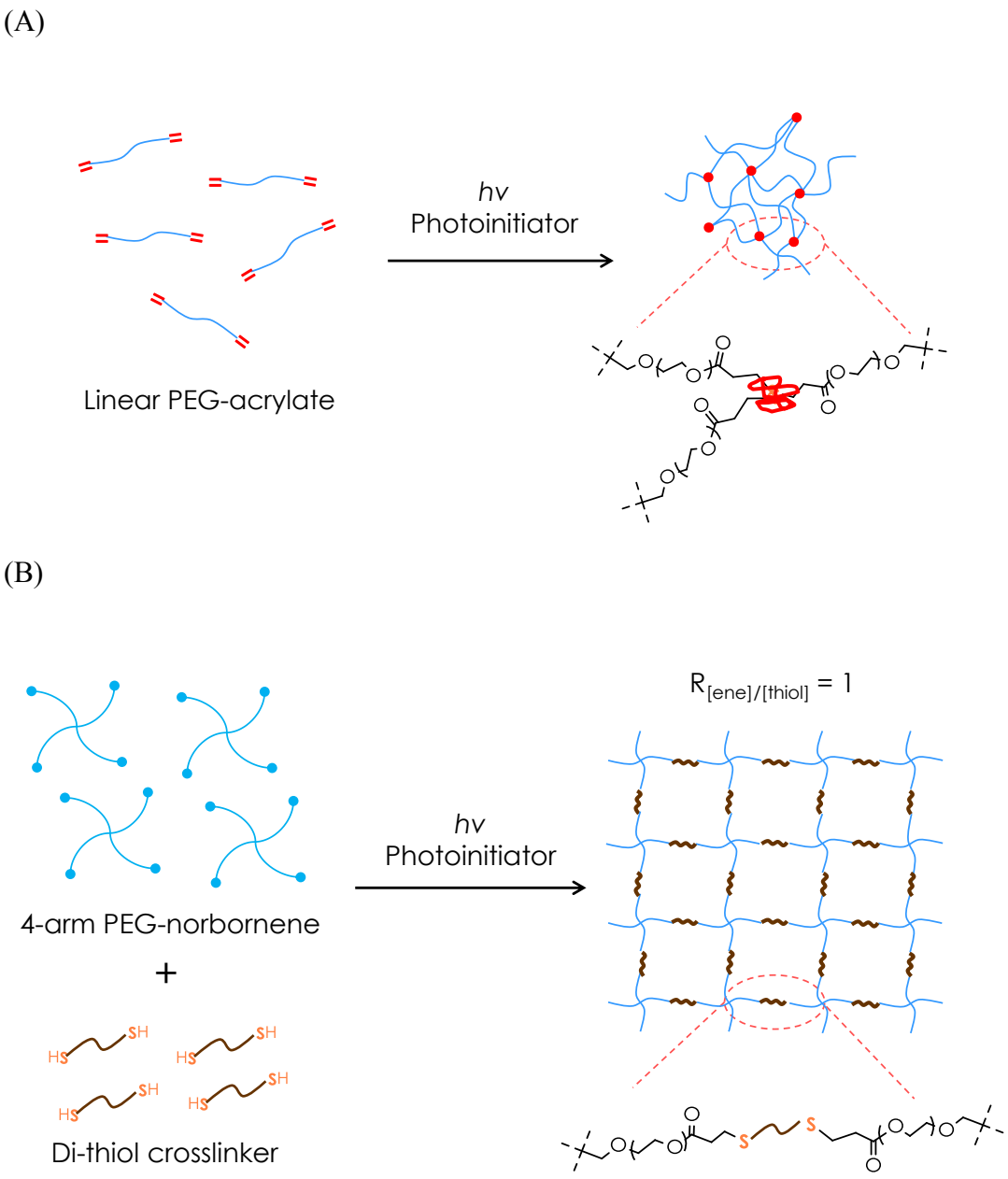

Figure 1.1 Schematics of hydrogels formed by: (A) Chain-growth photopolymerization of linear PEG-acrylate. (B) Step-growth photopolymerization of 4-arm PEG-norbornene and di-thiol containing crosslinkers at a unity molar ratio.

Water solubility and molar absorptivity at cytocompatible wavelengths are commonly used to evaluate the suitability of a photoinitiator to initiate photopolymerization for hydrogel synthesis. Only a few photoinitiators are considered cytocompatible, including type I initiators Irgacure-2959 (I-2959, Figure 1.2A) [12, 13] and lithium arylphosphanate (LAP, Figure 1.2B) [14], as well as type II initiator eosin-Y [10, 11, 15]. Commercially available I-2959 has low water solubility (< 0.5 wt%) and low molar absorptivity at 365 nm ($\varepsilon < 10\ M^{-1}cm^{-1}$). Added to these limitations is the fact that I-2959 cannot be used for visible light-mediated photocrosslinking due to its near zero molar absorptivity at wavelengths higher than 400 nm. While LAP is highly water-soluble (> 5 wt%) and has high absorbance at 365 nm ($\varepsilon \sim 200\ M^{-1}cm^{-1}$), its utility in visible light range is also very limited ($\varepsilon \sim 30\ M^{-1}cm^{-1}$ at 405 nm) [14]. Type II photoinitiator eosin-Y (Figure 1.2C), on the other hand, is highly water-soluble and can be readily excited by visible light ($\varepsilon > 100{,}000\ M^{-1}cm^{-1}$ at 516 nm). An example of this type of gelation is the synthesis of chain-growth poly(ethylene glycol) diacrylate (PEGDA) hydrogels. Unfortunately, a co-initiator (e.g., triethanolamine (TEOA, Figure 1.2D) and a co-monomer (e.g., 1-vinyl-2 pyrrolidinone (NVP, Figure 1.2E) are required for generating sufficient radicals to achieve high and rapid functional group conversion. This prerequisite makes adjusting the compositions of a macromer precursor solution complicated and is perhaps the main reason why UV-mediated photopolymerizations, even with biosafety concerns, is still a preferred method for preparing hydrogels.

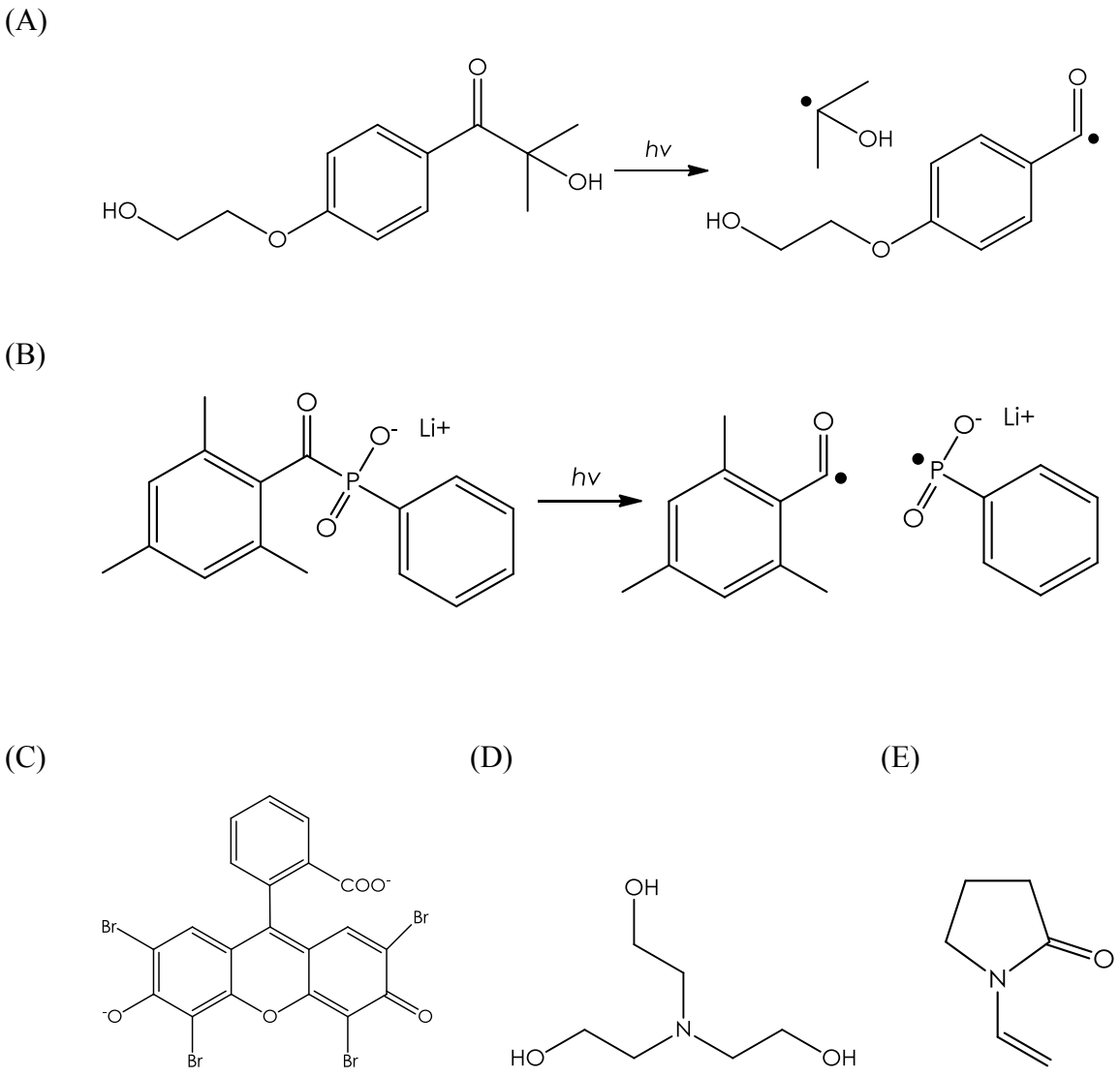

Figure 1.2 Photo-cleavage of type I (A) I-2959 and (B) LAP photoinitiator into radicals. Conventional type II photoinitiator (C) eosin-Y requires (D) co-initiator TEOA and (E) co-monomer NVP to generate sufficient radicals.

To overcome the disadvantages facing hydrogels formed by chain-growth photopolymerizations, Anseth and colleagues recently introduced a new class of PEG-peptide hydrogels based on radical-mediated orthogonal thiol-ene photo-click reaction [1]. In this system, low intensity and long wavelength (5 – 10 mW/cm^2, 365 nm) ultraviolet light was used to generate thiyl radicals (from bis-cysteine-containing oligopeptides), which crosslinked with ene moieties on norbornene-functionalized 4-arm PEG (PEG4NB) to form a step-growth network (Figure 1.3). This reaction scheme preserves all advantages offered by photopolymerizations, including rapid, ambient, and aqueous reaction conditions, as well as spatial-temporal control over gelation kinetics. Step-growth thiol-ene photo-click reactions are not oxygen inhibited [2], thus yielding more rapid gelation kinetics compared to chain-growth photopolymerizations [3]. Comparing to a step-growth Michael-type gelation (Figure 1.4B), thiol-ene photo-click reactions have reduced disulfide bond formation due to radical-mediated cleavage [4], thus increasing the extent of crosslinking that results in higher mechanical properties at similar macromer contents [1]. Furthermore, the orthogonal and step-growth nature of norbornene-sulfhydryl reaction permits dynamic modification of hydrogel biochemical and biophysical properties in the presence of cells [1]. Several cell types have been encapsulated successfully by these PEG-peptide hydrogels, including human mesenchymal stem cells [5], fibroblasts [1, 6], fibrosarcoma [6], valvular insterstitial cells [7], and radical-sensitive pancreatic β-cells [3]. Enzymatically degradable peptides could also be utilized to crosslink thiol-ene hydrogels for enzyme-responsive controlled release applications [8, 9].

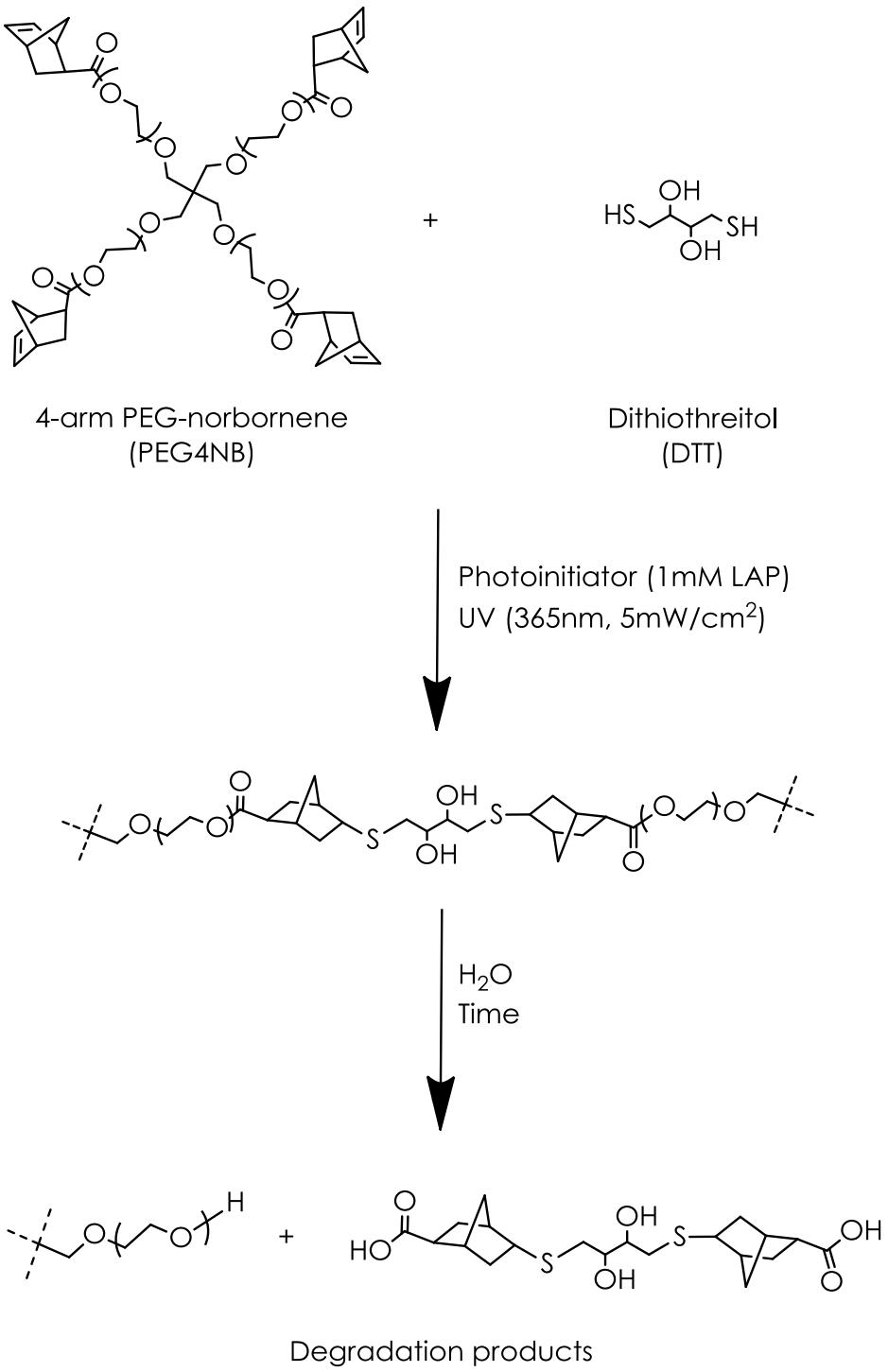

Figure 1.3 Schematics of photopolymerization and hydrolytic degradation of step-growth thiol-ene hydrogels. PEG-tetra-norbornene (PEG4NB) reacts with a bi-functional crosslinker DTT (dithiothreitol), in a step-growth manner, to form thioether linkage and crosslinked hydrogels. Hydrolytic degradation of the network occurs due to ester bond hydrolysis.

1.2 Degradable Hydrogels for Tissue Engineering Applications

An ongoing effort in biomaterial science and engineering is to design hydrogels with tunable and predictable degradation behaviors, because degradable hydrogels are particularly useful as provisional matrices for tissue regeneration and as carriers for controlled protein delivery [10-13]. Among all degradation mechanisms, hydrolytic degradation of synthetic hydrogels has received significant attention due to the simplicity of hydrolysis mechanism and well-defined polymer chemistry [14-16]. A classical way of preparing hydrolytically degradable hydrogels is by chain-growth photopolymerization of acrylated macromers, such as poly(lactic acid)-*b*-poly(ethylene glycol)-*b*-poly(lactic acid) (PLA-*b*-PEG-*b*-PLA) tri-block copolymers that hydrolyzed to form lactic acid, PEG and poly-acrylate (Figure 1.4A) [14, 17]. The hydrolytic degradation rate of these hydrogels could be tuned and predicted by using copolymers with different lengths of lactide repeating units [15, 16]. Similarly, other hydrolytically labile ester bonds could be incorporated to the termini of PEG macromers prior to acrylation or methacrylation [18, 19].

In addition to the chain-growth polymerized hydrogels, step-growth polymerized gels could also be rendered hydrolytically degradable. For example, Hubbell and co-workers developed Michael-type addition hydrogels through nucleophilic reactions between acrylates on multi-arm PEG macromer and sulfhydryl groups on the crosslinkers [20, 21]. Thioether-ester linkages formed between acrylate and sulfhydryl moieties were hydrolytically labile and the degradation rates of these hydrogels could be tuned by controlling macromer concentration and functionality (Figure 1.4B) [20, 22, 23]. Bowman and colleagues performed experimental and theoretical investigations on hydrolytic degradation of step-growth thiol-acrylate and thiol-allylether photopolymers [24-27]. Degradation was readily tuned and predicted using monomers with different concentration, functionality, and degradability. More recently, Leach and colleagues developed hydrolytically degradable Michael-type hydrogels based on 4-arm PEG-vinylsulfone (PEGVS) and PEG-diester-dithiol [28, 29]. Degradation of these step-growth hydrogels was altered by tuning the number of methylene groups between the

thiol and ester moieties in the PEG-diester-dithiol linkers. In the above examples, acidic by-products (i.e., carboxylic acid) are obtained from the ester hydrolysis mechanism.

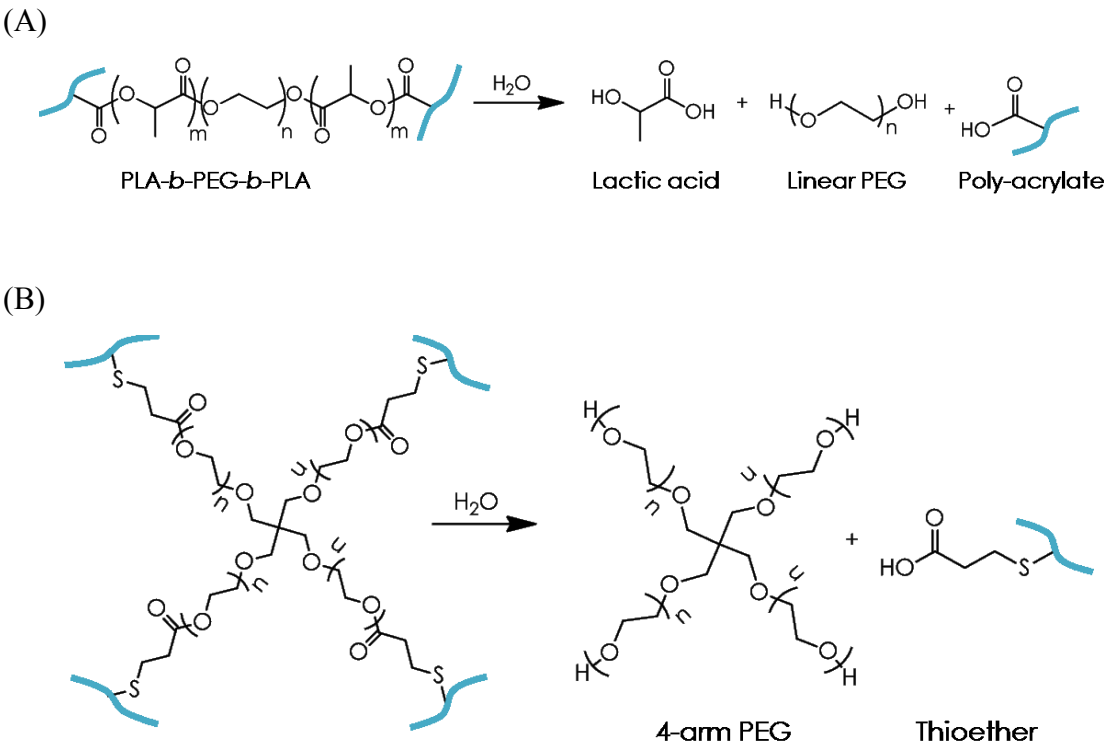

Figure 1.4 Schematics of hydrolytic degradation of: (A) chain-growth hydrogel formed by homopolymerization of PLA-*b*-PEG-*b*-PLA tri-block copolymer. (B) Step-growth Michael-type hydrogel formed by PEG-tetra-acrylate and di-thiol containing crosslinkers. Degradation occurs at the ester bonds on the PLA blocks and at the thioether-ester bonds.

While these degradable hydrogels have found various successful applications, limitations and challenges exist. For instance, chain-growth photopolymerized hydrogels are known to form dense hydrophobic polyacrylate chains [30] that yield network heterogeneity and high molecular weight degradation products [14-16]. On the other hand, the formation of step-growth Michael-type hydrogels often requires long gelation time that leads to the formation of high degrees of network defects [22]. It has been shown that high macromer functionalities (e.g., 8-arm PEG-acrylate) and concentrations (e.g., > 50 wt%) were necessary for step-growth Michael-type addition hydrogels to approach an 'ideal' network structure [22].

Although, in recent years, thiol-ene photopolymerized hydrogels discussed in previous section have emerged as an attractive class of biomaterials, the structure-property relationships of these hydrogels have not been extensively characterized. For example, an 'ideal network' was often mentioned in previous publications even with the use of low macromer concentrations (2 wt% to 10 wt% of PEG4NB) [1, 5, 8]. Furthermore, these thiol-ene hydrogels are susceptible to hydrolytic degradation due to the presence of an ester bond between the cyclic olefin and PEG backbone (Figure 1.3).

1.3 Multilayer Polymeric Biomaterials for Tissue Engineering Applications

Polymeric biomaterials with multilayer structures have great potential in biomedical applications, such as construction of complex tissues [31, 32], controlled release of multiple drugs at different rates [33-38], and immunoisolation for allo- or xeno-grafts [39, 40]. Many physical and chemical cross-linking methods have been developed for fabricating multilayer polymers or hydrogels. For example, polyelectrolytes with opposite charges could be self-assembled into multilayer films or membranes [34, 36, 37, 41]. These layer-by-layer (LbL, Figure 1.5A) approaches have been used successfully in producing films with nano-scale thickness for applications such as controlled drug delivery and cell surface coating [34, 37, 42]. However, the building blocks for LbL films usually comprise positively charged polymers that are potentially cytotoxicity. Further, the LbL assembly processes are often lengthy and may not be ideal for encapsulating sensitive cells. Other disadvantages include limitations in bioconjugation and drug loading capacity, as well as instability of the physically bonded films *in vivo*. The utility and diversity of multilayer biomaterials would greatly benefit from a chemically cross-linking method that provides long-term material stability, simplicity in coating procedures, and diversity in bioconjugation.

An attractive method to fabricate stable multilayer polymers or hydrogels is photopolymerization. This is because photopolymerization offers many benefits, including rapid and mild cross-linking conditions, as well as spatial-temporal control in

polymerization kinetics that permits the creation of complex material structures and functionalities [1, 13, 43]. A common approach to fabricate multilayer hydrogels is to prepare a layer of gel with pendent (meth)acrylate moieties that serve as anchors for subsequent homopolymerization of (meth)acrylated monomers (Figure 1.5B) [44, 45]. Either UV or visible light could be used to cross-link multilayer polymers, as long as appropriate initiator species are included in the subsequent monomer solutions. On the downside, current photopolymerization systems for forming hydrogels carry risks of cellular damages caused by UV light, radical species, and other cytotoxic compositions required in cross-linking reactions. Furthermore, currently available photochemistries for forming multilayer hydrogels are all based on chain-growth polymerizations that may not be ideal for some cell and protein encapsulation [3, 46].

Multilayer hydrogels could be fabricated using a light-independent approach. For instance, Bowman and colleagues have developed an enzymatic coating procedure for forming multilayer hydrogels (Figure 1.5C) [47-49]. The formation of hydrogel coating on a core gel was mediated by glucose oxidase (GOx), which reacts with its substrate glucose released from a core gel to generate hydrogen peroxide (H_2O_2). Hydrogen peroxide further reacts with ferrous ions (Fe^{2+}) to generate hydroxyl radicals, which initiate chain-growth polymerization through vinyl monomers. To control thickness of the hydrogel coating, one could simply control the reaction time or adjust concentrations of various components in the monomer solutions [48, 49]. However, since this polymerization method is light-independent, it also loses the benefits of photopolymerizations. Another disadvantage of this method is that a total of three initiating species (glucose oxidase, glucose, Fe^{2+}) are required, which complicate material preparation. Finally, this enzymatic reaction produces highly cytotoxic H_2O_2 and requires the addition of a second enzyme, catalase, to increase the cytocompatibility of this method for cell encapsulation [47].

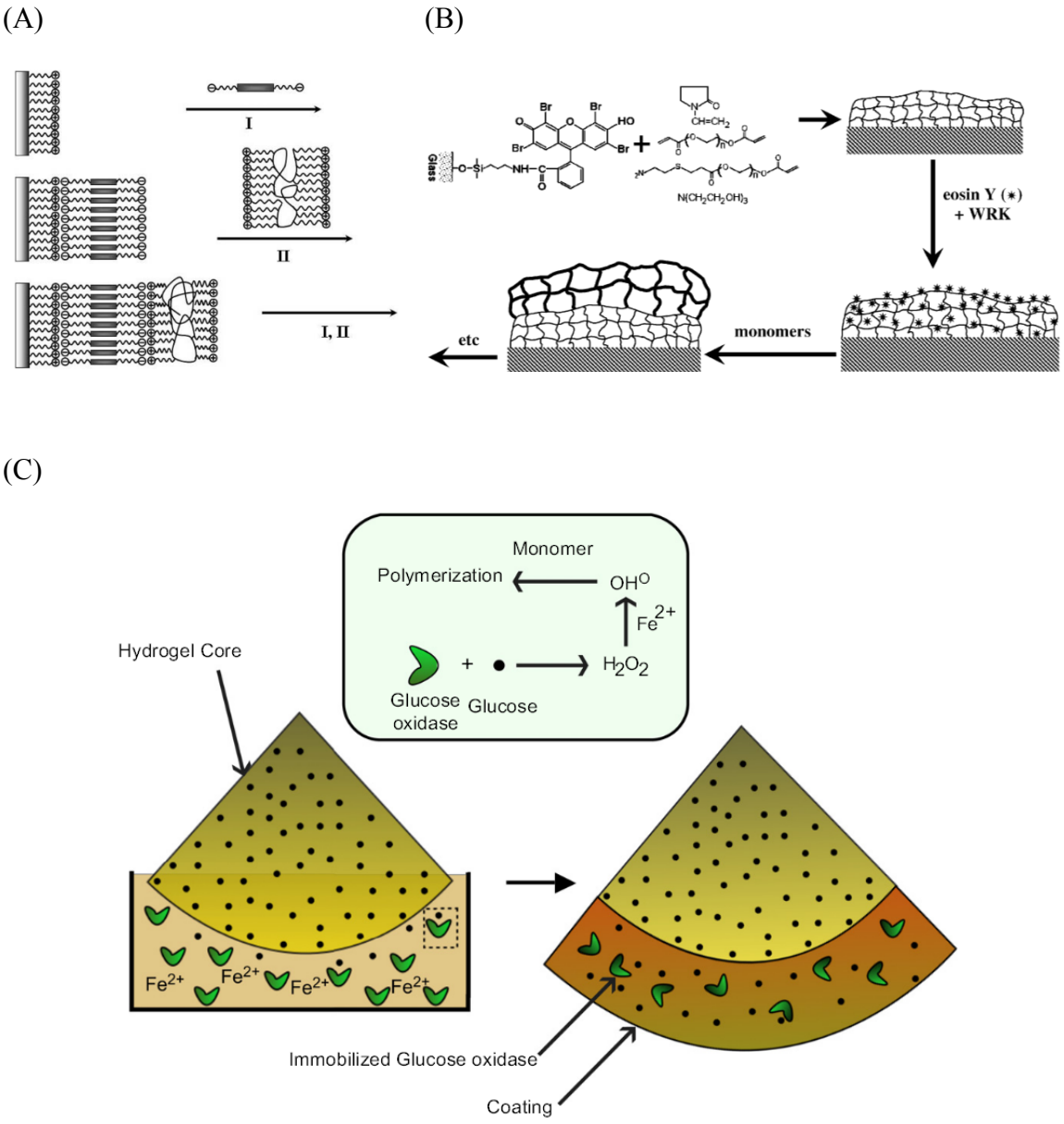

Figure 1.5 Approaches to form multilayer hydrogels. (A) Layer-by-layer (LbL) [41], (B) light-dependent homopolymerization of immobilized (meth)acrylated moieties [44] and (C) light-independent enzymatic coating [49]. Schemes were obtained from cited references.

2. OBJECTIVES

2.1 Overview

While step-growth thiol-ene photopolymerization has been widely used for tissue engineering and controlled release applications, the network ideality and degradation behaviors are not well described in literatures. Furthermore, the existing studies restricted the utility of thiol-ene photo-click chemistry to the use of UV light and a type I photoinitiator. The combination of a UV light source and a cleavage type photoinitiator often raise biosafety concerns. Therefore, a mild visible light source and a type II photoinitiator appear as an attractive alternative. In a conventional photopolymerization involving a type II photoinitiator, potentially cytotoxic co-initiator and co-monomer are required to achieve rapid gelation. The addition of these co-initiating species complicates the gelling mechanism and offsets the advantages of using visible light. To overcome the above mentioned limitations of the current thiol-ene hydrogelation, three specific aims are proposed.

2.2 Specific Aim 1: Characterize Thiol-ene Hydrogel Network Ideality and Degradability

This aim focuses on characterizing network crosslinking efficiency of thiol-ene hydrogels as compared to Michael-type addition hydrogels. Hydrogels rheological properties and swelling were measured to reveal gel network ideality. Hydrolytic degradation of thiol-ene hydrogels was systematically studied through experimental efforts and theoretical modeling. In addition, thiol-ene hydrogels network ideality and degradability were manipulated by using different macromer concentrations and peptide crosslinkers.

2.3 Specific Aim 2: Develop a Visible Light-mediated Thiol-ene Photo-click Mechanism

This aim focuses on developing a visible light-mediated thiol-ene hydrogels by using eosin-Y as the only photoinitiator to yield efficient gelation. This work also attempts to examine the cytocompatibility of these thiol-ene hydrogels using human mesenchymal stem cells (hMSCs) and sensitive pancreatic MIN6 β-cells using long-term viability assays and confocal imaging of cell viability using live/dead staining kit.

2.4 Specific Aim 3: Establish a New Approach to Form Multilayer Thiol-ene Hydrogels

This aim focuses on examining the re-excitability of eosin-Y for initiating sequential photocrosslinking. This work also aims to develop a simple experimental setup for forming multilayer hydrogels.

3. MATERIALS AND METHODS

3.1 Materials

4-arm PEG-OH (20 kDa) and 4-arm PEG-amine (20 kDa) were purchased from JenKem Technology USA. Fmoc amino acids and coupling reagents for peptide synthesis were acquired from Anaspec. Eosin-Y disodium salt, TEOA and NVP were purchased from Fisher Scientific. Linear PEG (10 kDa) and all other chemicals were obtained from Sigma-Aldrich unless noted otherwise.

3.2 PEG Macromers and Photoinitiator Synthesis

Poly(ethylene glycol)-tetra-norbornene (PEG4NB) and PEG-di-norbornene (PEGdNB) were synthesized using an established protocol [1, 5]. A day before the synthesis, required glassware and measured PEG-OH (4-arm or linear) were placed in oven (at 120 ^{o}C) and vacuum oven (at 37 ^{o}C and 25 mmHg) to dry, respectively. Briefly, norbornene anhydride was formed by reacting 5-norbornene-2-carboxylic acid and coupling reagent N,N'-dicyclohexylcarbodiimide (DCC) in anhydrous dichloromethane (DCM) for 1 hour at room temperature under constant nitrogen gas purging. The latter was filtered through a fritted funnel into a second flask containing PEG-OH (8-arm, 4-arm or linear), 4-(dimethylamino)pyridine (DMAP), and pyridine in anhydrous DCM. After overnight reaction, the product was washed with 5 vol% sodium bicarbonate solution twice, 5 vol% of hydrochloric acid and brine once, followed by precipitation in cold ethyl ether (on an ice bath). The product was then filtrated, re-dissolved in minimum amount of DCM, and re-precipitated in cold ethyl ether. ^{1}H NMR (Bruker Avance III 500) was used to confirm the degree of PEG functionalization (> 90 %, Appendix A).

Poly(ethylene glycol)-tetra-amide-norbornene (PEG4aNB) was synthesized by reacting norbornene acid (5-fold excess to amine groups) with PEG-tetra-amine in DMF using HBTU/HOBT as coupling reagents. After overnight reaction at room temperature, the product was precipitated in cold ethyl ether and purified with the same protocol for PEGNB purification. ^{1}H NMR (Bruker Avance III 500) was used to confirm the degree of PEG functionalization (> 90 %, Appendix B).

Poly(ethylene glycol)-tetra-acrylate (PEG4A) and poly(ethylene glycol)-di-acrylate (PEGDA) were synthesized following an established protocol. PEG-OH (4-arm or linear) were dried in toluene using azeotropic drying method for 2 hours under nitrogen. In an addition funnel, acryloyl chloride was dripped slowly to the round flask containing dried PEG-OH (4-arm or linear) with triethylamine (TEA). After overnight reaction, the solution was filtered through a thin layer of neutral aluminum oxide. Sodium carbonate was added to the solution and the heterogeneous solution was stirred for 2 hours in the dark. The solution was then filtered through Hyflo filtration aid, rotovap to reduce solvent volume and the clear solution obtained was precipitated in cold ether. High degree of PEG functionalization (> 90 %, Appendix C) was confirmed by ^{1}H NMR (Bruker Avance III 500).

The synthesis of photoinitiator lithium arylphosphinate (LAP) was described as reported elsewhere [50]. In brief, an equal amount of 2,4,6-trimethylbenzoyl chloride was added slowly to the round bottom flask containing desired amount of dimethyl phenylphosphonite. The setup was purged with nitrogen at room temperature until the completion of dripping 2,4,6-trimethylbenzoyl chloride. After overnight reaction, 4-molar excess of lithium bromide in 2-butanone was added to the reaction mixture which was heated to 50 °C. Solid precipitates of lithium phenyl-2,4,6-trimethylbenzoylphosphinate were formed after 10 minutes. The product was cooled to room temperature and maintained for 4 hours. To purify the product, the mixture was filtered through a fritted funnel, washed with 2-butanone for 3 times, and washed with cold ethyl ether to remove

unreacted lithium bromide. 1H NMR prediction (500 MHz, D_2O, δ): 7.57 (m, 2H), 7.42 (m, 1H), 7.33 (m, 2H), 6.74 (s, 2H), 2.09 (s, 3H) and 1.88 (s, 6H). (Appendix D)

3.3 Microwave Assisted Solid-Phase Peptide Synthesis (SPPS)

All peptides were synthesized following the process of Fmoc Solid Phase Peptide Synthesis (SPS) with a microwave peptide synthesizer (CEM Discover SPS). A condensed version of a peptide synthesis procedure involved: swelling, deprotection, coupling, cleavage and washing. First, Fmoc-Rink-amide-MBHA resin was swelled in dimethylformamide (DMF) for 15 minutes. Second, deprotection procedures (in 20 % piperidine/DMF with 0.1 M HOBt) were performed in the microwave for 3 minutes at 75 ^{o}C with microwave power set at 20 W. Third, 5-fold molar excess of Fmoc-protected amino acids with HBTU (5-fold molar excess) were dissolved in an activation solution (0.28 M DIEA in DMF). This dissolved solution was added to the deprotected resin to perform coupling using the microwave for 5 minutes at 75 ^{o}C and 20 W. To reduce racimification, cysteine was coupled at 50 ^{o}C with the same procedure for 10 minutes. Nihydrin test was conducted after each deprotection or coupling procedure to ensure complete removal of Fmoc (negative result) or coupling of amino acid (positive result). In the final stage, peptide was cleaved from the resin in a 5 mL of cleavage cocktail solution (95 vol% trifluoroacetic acid – TFA, 2.5 vol% triisopropylsilane – TIPS, 2.5 vol% distilled water and 250 mg of phenol) in the microwave for 30 minutes at 38 ^{o}C and 20 W. Peptide product was precipitated in cold ether, dried in vacuuo and stored in -20 ^{o}C. HPLC (PerkinElmer Flexar system) was used to purify peptide (> 90 %), and mass spectrometry (QTOF, Agilent Technologies) was used to confirm the peptide sequence. Furthermore, Ellman's assay (PIERCE) was used to quantify the concentrations of the prepared stock solution by quantifying the sulfhyldryl group.

3.4 Hydrogel Fabrication

Step-growth thiol-ene hydrogels were formed by radical-mediated photopolymerization between macromer (i.e., PEG4NB) and di-thiol containing crosslinkers, such as dithiothreitol (DTT) or cysteine-containing peptides (Figure 1.3). Unless otherwise stated, a unity molar ratio between thiol and ene groups was used. Thiol-ene photopolymerization was initiated by either 1 mM LAP under ultraviolet light exposure (365 nm, 5 mW/cm^2) for 3 minutes or 0.1 mM eosin-Y under visible light exposure (400 to 700 nm, 70,000 Lux) for 4 minutes in buffer solutions. Step-growth Michael-type hydrogels were formed from PEG4A and DTT (at stoichiometric ratio) in a humidified oven (37 ^{o}C) for overnight to ensure complete gelation at pH 8.0. Chain-growth visible light-mediated PEGDA hydrogels were formed by radical-mediated photopolymerization using 0.1 mM of eosin-Y under visible light exposure at an intensity of 70,000 Lux using a fiber optic microscope illuminator (AmScope). Co-initiator (0.75 vol% of TEOA) and co-monomer (0.1 vol% NVP) were added in PEGDA precursor solution.

3.5 Hydrogel Swelling

For swelling studies, each gel was prepared from 50 μL precursor solution. After gelation, hydrogels were incubated in ddH_2O at 37 ^{o}C on an orbital shaker for 48 hours to remove uncrosslinked (sol fraction) species. Gels were then dried and weighed to obtain dried polymer weights (W_{Dry}). The dried polymers were then incubated in 5 mL of buffer solution (pH 6.0, pH 7.4 or pH 8.0 PBS) at 37 ^{o}C on an orbital shaker. At pre-determined time intervals, hydrogels were removed from the medium, blotted the gel surface with Kimwipe tissue, and weighed to obtained swollen weights ($W_{Swollen}$). Hydrogel mass swelling ratios (q) at equilibrium were defined as:

$$q = \frac{W_{Swollen}}{W_{Dry}} \tag{3.1}$$

As described by Metters *et al*. [15, 16], the mass swelling ratio (q) of a hydrolytically degrading network increases exponentially as a function of degradation time:

$$q = q_0 e^{-k_{hyd} t} \tag{3.2}$$

Here, q_0 represents the initial mass swelling ratio before significant occurrence of degradation and k_{hyd} is the apparent pseudo first-order ester hydrolysis rate constant, which was obtained via exponential curve fitting to the experimental swelling data.

To quantify hydrogel swelling, circular hydrogel discs were prepared from 50 μL precursor solution. Immediately after gelation, hydrogels were incubated in ddH_2O at 37 ^oC on an orbital shaker for 24 hours to remove sol fraction. Gels were then dried and weighed to obtain dried polymer weights (W_{Dry}). The dried polymers were incubated in 5 mL of buffer solution (pH 7.4 PBS) at 37 ^oC on an orbital shaker. At equilibrium swelling (after 48 hours), hydrogels were removed from the medium, blotted dry with Kimwipe, and weighed to obtain swollen weights ($W_{Swollen}$). Hydrogel mass swelling ratios (q) were determined by a ratio of $W_{Swollen}$ to W_{Dry}.

3.6 Rheometry

For rheometrical property measurements, hydrogel slabs were fabricated between two glass slides separated by 1 mm thick spacers. Circular gel discs (8 mm in diameter) were punched out from the gel slabs using a biopsy punch and placed in pH 7.4 PBS for 48 hours. Strain sweep (0.1 % to 20 %) oscillatory rheometry was performed on a Bohlin CVO 100 digital rheometer. Shear moduli of the hydrogels were measured using a parallel plate geometry (8 mm) with a gap size of 800 μm. Tests were performed in the linear viscoelastic region (LVR).

In situ gelation rheometry for thiol-ene hydrogels was conducted in a light cure cell at room temperature. Briefly, the macromer solution was placed on a quartz plate in the light cure cell, and irradiated with UV light (Omnicure S1000, 365 nm, 5 mW/cm^2)

through a liquid light guide or a fiber optic microscope illuminator (AmScope, 400 to 700 nm, 70,000 Lux). *In situ* gelation rheometry for Michael-type hydrogels was measured at 37 ^{o}C using an 8 mm parallel plate geometry. Time sweep *in situ* rheometry was performed with 10 % strain, 1 Hz frequency, 0.1 N normal force, and a gap size of 100 μm. Gel point (i.e., crossover time) was determined at the time when storage modulus (G') surpassed loss modulus (G").

3.7 Network Structure of Step-growth Hydrogels

A perfectly crosslinked (or 'ideal') thiol-ene or Michael-type hydrogel network without defects can be estimated by means of hydrogel equilibrium swelling [22]. Considering the structural information of the step-growth hydrogels (i.e., macromer molecular weight and functionality), the average molecular weight between crosslinks ($\overline{M_c}$) is defined as [22]:

$$\overline{M_c} = 2\left(\frac{MW_A}{f_A} + \frac{MW_B}{f_B}\right) \tag{3.3}$$

Here, MW_A and MW_B represent the molecular weight of PEG4NB and crosslinker, respectively. f_A and f_B are the number of reactive functionality for PEG4NB (or PEG4A) and crosslinker. With a known $\overline{M_c}$, the ideal network crosslinking density or density of elastically active chains (v_c) and polymer volume fraction (v_2) can be calculated based on the Flory-Rehner theory [51]:

$$v_c = \frac{V_1}{\overline{M_c}\,\overline{v_2}} = \frac{-\left[\ln(1-v_2) + v_2 + \chi_{12}\, {v_2}^2\right]}{{v_2}^{1/3} - \frac{2\,v_2}{f_A}} \tag{3.4}$$

Here, $\overline{v_2}$ is the specific volume of PEG (0.92 cm^3/g at 37 ^{o}C), V_1 is the molar volume of water (18 cm^3/mole) and χ_{12} is the Flory-Huggins interaction parameter for a PEG-H_2O system (0.45). After obtaining v_2, ideal hydrogel mass swelling ratio q can be obtained using the following equation:

$$v_2 = \frac{\overline{v_2}}{(q-1)\,\overline{v_1} + \overline{v_2}} \tag{3.5}$$

where $\overline{v_1}$ is the specific volume of water (1.006 cm^3/g at 37 ^{o}C).

3.8 Prediction of Hydrolytic Degradation of Thiol-ene Hydrogel

The statistical-*co*-kinetic model established by Metters and Hubbell for predicting the hydrolytic degradation of step-growth hydrogels takes into account of ester bond hydrolysis kinetics and the structural information such as the connectivity of the ideal hydrogel networks. Based on this model, the degradation of thiol-ene hydrogels was assumed to be purely due to ester bond hydrolysis with a pseudo-first order degradation kinetics [15, 16]. With this assumption, the fraction of hydrolyzed ester bonds (P_{Ester}) at any given time in the system is expressed as:

$$P_{Ester} = 1 - \frac{[Ester]}{[Ester]_0} = 1 - e^{-k't} \tag{3.6}$$

Here, *k'* is the pseudo-first order ester bond hydrolysis rate constant. [Ester] and $[Ester]_0$ are the current and initial numbers of intact ester bonds in the system.

The fraction of intact elastic chains (i.e., crosslinkers such as DTT or bis-cysteine containing peptides) within these crosslinked networks at any given time is expressed as:

$$1 - P_{Chain} = (1 - P_{Ester})^N = e^{-Nk't} \tag{3.7}$$

where N is the number of degradable units (i.e., ester bonds) connected to one elastic chain (e.g., N = 2 for the case of PEG4NB-DTT hydrogels).

To obtain the degree of crosslinking in the system, one must also consider the connectivity of multi-arm PEG macromers. For an ideal step-growth network, the fraction of f_A-armed macromer with i arms still connected to the network at any time point during ester hydrolysis is expressed as:[13]

$$F_{i,f_A} = \frac{f_A!}{(f_A - i)!i!} P_{chain}^{(f_A - i)}(1 - P_{chain})^i \tag{3.8}$$

With this information, the crosslinking density of the degrading network is expressed as:

$$v_c = (\sum_{i=3}^{f_A} \frac{i}{2} F_{i,f_A})[A]_0 \tag{3.9}$$

Here, $i \geq 3$ because any f_A-arm ($f_A \geq 3$) macromer with only two arms connected to intact elastic chains forms an extended loop, rather than a crosslink. $[A]_0$ represents the

concentration of f_A-arm macromers (e.g., PEG4NB) in the equilibrium swelling state before the onset of network degradation, which is correlated to the crosslinking density of a network:

$$v_{c,0} = \frac{f_A}{f_B} [A]_0 \quad (3.10)$$

When the functionalities of the macromer and crosslinker (f_A = 4 and f_B = 2) are taken into account, the crosslinking density of a perfectly crosslinked thiol-ene network in the equilibrium state could be derived from Equations 3.4 to 3.10 and expressed as:

$$v_c = (6e^{-3Nk't} - 4e^{-4Nk't}) [A]_{0,actual} \quad (3.11)$$

For gels with non-idealities, based on Equations 3.4, 3.5, and 3.11, $[A]_{0,actual}$ is obtained using actual crosslinking density as:

$$[A]_{0,actual} = \frac{v_{c,actual}}{v_{c,ideal}} [A]_0 \quad (3.12)$$

where $v_{c,actual}$ represents the experimental crosslinking density converted from experimental mass swelling ratio using Equations 3.4 and 3.5 and $v_{c,ideal}$ represent ideal crosslinking density calculated based on $\overline{M_c}$ derived from Equation 3.3.

3.9 Enzymatic Degradation

4 wt% PEG4NB hydrogels (30 μL/gel) were crosslinked by bis-cysteine containing peptides with different percentages of chymotrypsin-sensitive (CGGY↓C: arrow indicates cleavage site) and non-sensitive (CGGGC) sequences. Hydrogels were fabricated using methodology described above and incubated in 500 μL PBS containing 0.5 mg/mL of chymotrypsin at room temperature on an orbital shaker. At specific time points, hydrogels were removed from the chymotrypsin solution, blotted dry, measured the swollen mass, and placed back into the chymotrypsin solution. Fresh chymotrypsin solution was prepared every 15 minutes to ensure enzyme activity. Percent mass loss is defined as:

$$Mass\ loss\ (\%) = \frac{W_t - W_0}{W_0} \times 100\% \quad (3.13)$$

where W_t is the gel weight measured at specific time points and W_0 is the mass measured at equilibrium swelling (48 hours).

In a separate experiment, 4 wt% of PEG4NB hydrogels were crosslinked by CGGYC and CGGDC at a percent molar ratio of 20 to 80 %. These gels were incubated in pH 7.4 PBS that was changed every two days. At specific time point, these gels were treated with chymotrypsin solution for 30 minutes on an orbital shaker. Fresh chymotrypsin solution was prepared every 15 minutes to ensure enzyme activity. After the chymotrypsin treatment, the hydrogels were washed with chilled (4 ^{o}C) PBS for 1 hour to deactivate enzyme activity. These gels were incubated in pH 7.4 PBS at 37 ^{o}C for swelling study.

3.10 Cell Encapsulation

To study the cytocompatibility of type II initiator, eosin-Y, desired density (5×10^6 cells/mL) of hMSCs or mouse insulinoma cells (MIN6, 2×10^6 cells/mL) were suspended in the following sterile polymer precursor solutions: (1) PEG4NB and DTT; (2) PEG4aNB and DTT; or (3) PEGDA, TEOA, and NVP. All precursor solutions contained 0.1 mM of eosin-Y and 0.1 mM of CRGDS for hMSCs encapsulation. Precursor solutions (25 μl) were exposed with the same visible light source (70,000 Lux) for 4 minutes at room temperature. hMSCs cell-laden hydrogels were incubated in low-glucose DMEM supplemented with 10 % fetal bovine serum (FBS, Gibco), 1 ng/mL basic fibroblast growth factor (bFGF, Peprotech), and 1 × antibiotic-antimycotic (Invitrogen) at 37 ^{o}C and 5 % of CO_2. MIN6 cell-laden hydrogels (25 μl) were cultured in high-glucose DMEM supplemented with 10 vol% fetal bovine serum (FBS), 50 μM β-mercaptoethanol, and 1 × antibiotic-antimycotic.

To quantify long-term cell viability, cell-laden hydrogels were incubated in 500 μL Alamarblue® reagent (AbD Serotec, 10 % in cell culture medium) at 37 ^{o}C and 5 % of CO_2. After 14 hours of incubation, 200 μl of media were transferred to a 96-well plate

for fluorescence quantification (excitation: 560 nm and emission: 590 nm) using a microplate reader (BioTek, Synergy HT). In addition, at specific time points cell-laden hydrogels were stained with Calcein AM (0.25 μL/mL, stained live cells) and Ethidium homodimer-1, EthD, (2 μL/mL, stained dead cells) for confocal microscopy imaging (Olympus Fluoview, FV1000). Four images were taken per hydrogel and each Z-stack confocal image contained 11 slices with 10 μm increment per slice. The number of live and dead cells was counted separately per Z-stack image to determine percent cell viability, which is the number of live cells divided by the sum of live and dead cells.

3.11 Retention and Recovery of Eosin-Y in Hydrogels

Immediately after polymerization, hydrogel discs (8 mm diameter × 1 mm height) were immersed into scintillation vials containing 2 mL of PBS (pH 7.4) at 37 ^{o}C. At specific time points, a portion of solution (200 μL) was transferred to a clear 96-well plate and fresh PBS was added to maintain a constant volume (2 mL). Absorbance (516 nm) of the collected samples was measured by a microplate reader (BioTek Synergy HT) and correlated to a standard curve generated from known concentrations of fresh eosin-Y. Mass balance calculations were performed to determine the quantity of eosin-Y retained in the hydrogels. In a similar manner, eosin-Y was recovered from the buffer and the concentration was determined by absorbance measurement using eosin-Y solutions with known concentrations.

3.12 UV/Vis Absorbance of Eosin-Y Containing Samples

Eosin-Y and various components (i.e., DTT and PEGdNB) were dissolved in PBS (pH 7.4) and exposed to visible light for 4 minutes. Non-gelling macromers were used (e.g., PEGdNB) to prevent gelation and facilitate solution-based UV/Vis spectrometric measurements. Concentrations of the components were equivalent to those used in gelation studies. The spectra of the solutions were measured between 400 and 600 nm at 1 nm increment using a microplate reader (BioTek Synergy HT) in UV/Vis absorption

mode. Prior to measurements, the solutions were diluted down to equivalent of 0.02 mM eosin-Y to ensure that the absorbance values measured were within the linear range of a standard curve generated using known eosin-Y concentrations.

3.13 Multilayer Hydrogel Fabrication and Characterization

In the three-layer hydrogel experiment, all layers were formed with 10 wt% PEG4NB and DTT at a unity stoichiometric ratio. Gels were prepared in a 1 mL syringe with the tip cut off. The bottom layer was formed under visible light (70,000 Lux) for 4 minutes using 2.0 mM eosin-Y as the only photoinitiator. The macromer precursor solutions in the middle and top layers (25 μL each) contained only PEG4NB and DTT (5 % of 0.2 μm Fluoresbrite® blue microparticles in the top layer were added for visualization purpose). These layers were formed by sequential visible light exposure for 10 minutes each (200,000 Lux). The formation of the thick coating gel construct was achieved in a similar manner. A gel disc (2 mm diameter × 1 mm height) was pre-formed using 2 mM eosin-Y and placed in a 1 mL syringe filled with macromer solution (10 wt% PEG4NB and DTT). The set up was exposed under visible light through a gooseneck light guide (200,000 Lux) for 10 minutes.

3.14 Data Analysis

Data analysis and curve fitting were performed on Prism 5 software. The pseudo-first order rate constant (*k'*) was determined using Matlab 2010 built-in curve-fit tool function. A best-fit *k'* was determined based on Matlab built-in trust region algorithm with an R^2 value of 0.95 or greater. Unless otherwise noted, all experiments were conducted independently for three times and the results were reported as mean ± S.D..

4. RESULTS AND DISCUSSION

4.1 Step-growth Thiol-ene vs Michael-type Polymerization

The network ideality and hydrolytic degradation behaviors of step-growth thiol-ene hydrogels received little attention in previous reports. Given the attractive features offered by this new class of biomaterials, we were interested in characterizing and understanding these properties. In addition, while it has been suggested that thiol-ene photopolymerization produces hydrogels with higher degree of crosslinking when compared to Michael-type addition hydrogels, no direct experimental comparison has been made to verify this claim. Here, we prepared step-growth thiol-ene or Michael-type hydrogels using PEG4NB or PEG4A macromers. DTT was used as a hydrogel crosslinker for both systems. Since PEG4NB and PEG4A used in this study have the same molecular weight (MW_A = 20 kDa) and functionality (f_A = 4), hydrogels crosslinked by these macromers without any structural defect would have the same degree of crosslinking at identical macromer concentration (i.e., 4 wt%). Therefore, variations in hydrogel physical properties (e.g., swelling, modulus, and etc.) could be used to evaluate the network connectivity. We first characterized the gelation kinetics of these two step-growth hydrogel systems via *in situ* rheometry. As shown in Figure 4.1, the gel point of thiol-ene photo-click reaction was ~265-fold faster than that of Michael-type addition reaction (3 ± 1 vs 689 ± 18 seconds). While the time required to reach complete gelation for thiol-ene photo-click reaction was less than 3 minutes (Figure 4.1A), it took almost 25 – 30 minutes for the Michael-type reaction to reach complete gelation (Figure 4.1B). In addition, the final shear modulus (G') for thiol-ene hydrogels was one order of magnitude higher than that of Michael-type hydrogels (2030 ± 80 Pa vs 470 ± 20 Pa), indicating improved network connectivity in thiol-ene hydrogels.

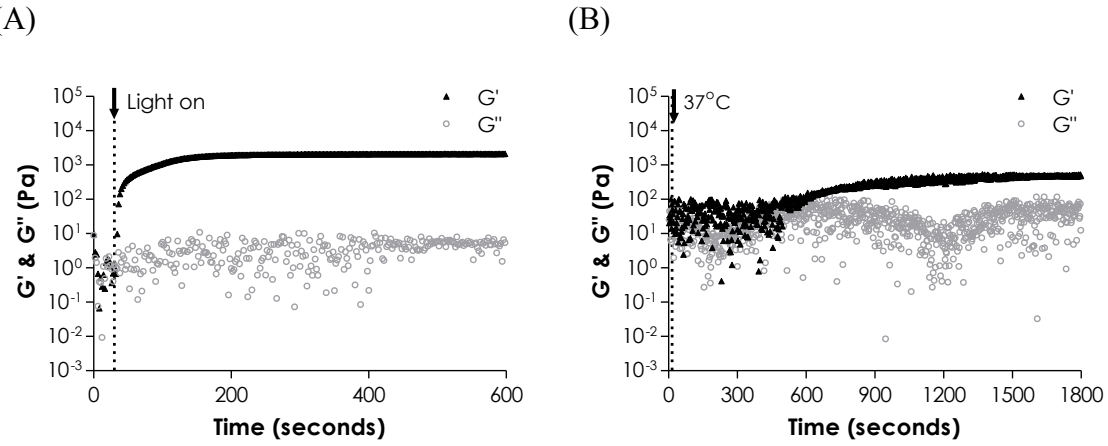

Figure 4.1 *In situ* rheometry of step-growth hydrogels: (A) Thiol-ene photo-click polymerization (4 wt% PEG4NB-DTT). UV light was turned on at 30 seconds (Dotted line). (B) Michael-type addition (4 wt% PEG4A-DTT). Dotted line at 15 seconds indicates temperature reached 37 ^{o}C.

We further compared these two gel systems using hydrogel equilibrium swelling and shear modulus, both of which are directly related to hydrogel crosslinking density [52]. Based on Equation 3.3, the molecular weight between crosslinks ($\overline{M_c}$) of these two step-growth hydrogel systems without defect should be identical (neglecting the minor difference in the molecular weight of norbornene and acrylate moiety) and was calculated as 10,154 Da. Accordingly, the ideal mass swelling ratio of a perfectly crosslinked step-growth hydrogel ($q_{eq,\,\text{ideal}}$) was calculated as 9.6 using Equations 3.4 and 3.5 (Table 4.1 and dashed line in Figure 4.2). Experimentally, however, we found that thiol-ene hydrogels, when compared to Michael-type gels at identical macromer compositions, had lower mass swelling ratio (28.5 ± 2.2 vs 44.5 ± 3.8) and higher elastic modulus (~1 vs ~0.2 kPa) at the equilibrium state. These experimental results confirmed a previous notion that radical-mediated thiol-ene reaction, when compared to Michael-type conjugation reaction, produce step-growth hydrogels with faster gelation kinetics, less structural defects, higher degree of crosslinking, and improved gel mechanical properties.

Table 4.1 Characteristics of step-growth Michael-type and thiol-ene hydrogels (4 wt%, 20 kDa, 4-arm PEG-derivatives crosslinked by DTT, pH 7.4, N = 4).

	$\overline{M_c}$ (Da)	$q_{eq,\ ideal}$	$q_{eq,\ actual}$	$G'_{eq,\ actual}$ (kPa)
PEG4A (Michael-type)	10,154	9.6	44.5 ± 3.8	0.2 ± 0.1
PEG4NB (Thiol-ene)	10,154	9.6	28.5 ± 2.2	1.1 ± 0.1

4.2 UV Light-mediated Thiol-ene Hydrogelation Using Photoinitiator LAP

4.2.1 Crosslinking Efficiency

As shown in Table 4.1, an 'ideal' step-growth network with a fixed macromer composition and without defect should only have a single equilibrium swelling ratio. Furthermore, the swelling ratio should be independent of macromer concentrations at equilibrium state. The experimental equilibrium mass swelling ratios of PEG4NB-DTT gels, however, exhibited high dependency on PEG4NB macromer concentration as shown in Figure 4.2. For example, when the concentration of PEG4NB macromer was increased from 4 wt% to 20 wt%, swelling ratios decreased from 28.5 ± 2.2 to 12.1 ± 0.2 and approached ideal equilibrium swelling ratio (9.6). Hydrogels with low swelling ratios (at higher macromer contents) had higher elastic moduli (~1 kPa and ~10 kPa for 4 wt% and 10 wt% PEG4NB-DTT hydrogels, respectively). This inverse relationship was commonly observed in chemically crosslinked networks, including chain-growth PEGDA hydrogels.

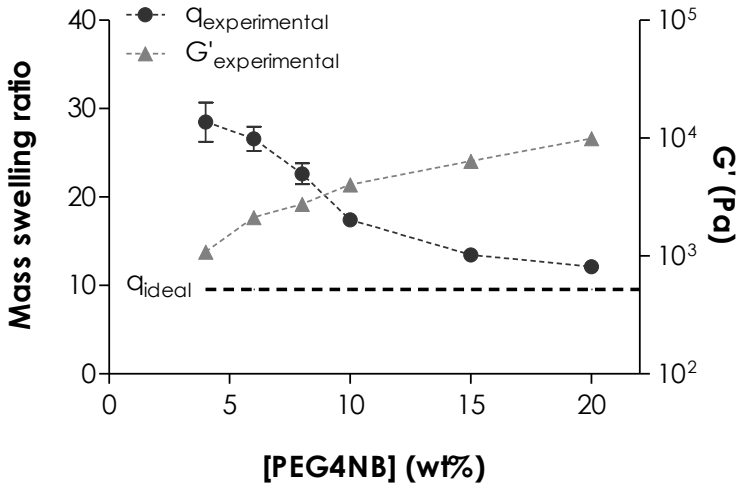

Figure 4.2 Effect of PEG4NB macromer concentration on hydrogel equilibrium swelling (left y-axis) and elastic modulus (right y-axis). Swelling ratio of an ideal network was calculated based on the molecular weight between crosslinks ($\overline{M_c}$) of given macromer molecular weights (MW_{PEG4NB} = 20 kDa, MW_{DTT} = 154 Da) and functionalities (f_{PEG4NB} = 4, f_{DTT} = 2).

The trend observed in Figure 4.2 could be attributed to a higher tendency of cyclization at lower PEG4NB contents. At diluted macromer concentrations, higher extent of intramolecular reactions led to formation of more primary cycles. Consequently, lower degree of intermolecular crosslinking resulted in increased gel swelling, and vice-versa [22]. The network defects resulted from different degrees of intramolecular and intermolecular reactions was the major reason for the dependency of experimental equilibrium swelling ratios on macromer concentrations [22].

The strong dependency between macromer concentration (especially at lower concentrations) and network ideality in thiol-ene hydrogels was beneficial in that the physical properties (e.g., swelling and modulus) of these thiol-ene hydrogels could be easily tuned for biological applications (Figure 4.2). For example, hydrogel shear moduli obtained (~1 to 10 kPa) using current thiol-ene hydrogel formulations were within a physiologically-relevant range and could be used to study the effect of matrix stiffness on cell fate processes [53, 54]. More importantly, the gelation time for these thiol-ene

hydrogels was drastically shortened when compared to the crosslinking of chain-growth PEGDA or step-growth Michael-type hydrogels.

4.2.2 Effect of pH on Degradation of PEG4NB-DTT Hydrogels

As stated previously, thiol-ene hydrogels could be degraded hydrolytically via ester hydrolysis. We found that the degradation of thiol-ene hydrogels was pH-dependent (Figure 4.3). PEG4NB-DTT hydrogels incubated in acidic condition (pH 6.0) were stable with an almost constant swelling ratio over a 45-day period, whereas hydrogels with the same compositions exhibited increasing swelling over time in slightly basic conditions (pH 7.4 and pH 8.0). We conducted exponential curve fittings using the swelling data of degrading hydrogels and found high degree of correlation between the fitted curves with the experimental data (dashed curves, $R^2 = 0.98$ for both pH 7.4 and pH 8.0 in Figure 4.3), indicating that the degradation of thiol-ene hydrogels was most likely a result of pseudo-first order ester bond hydrolysis.

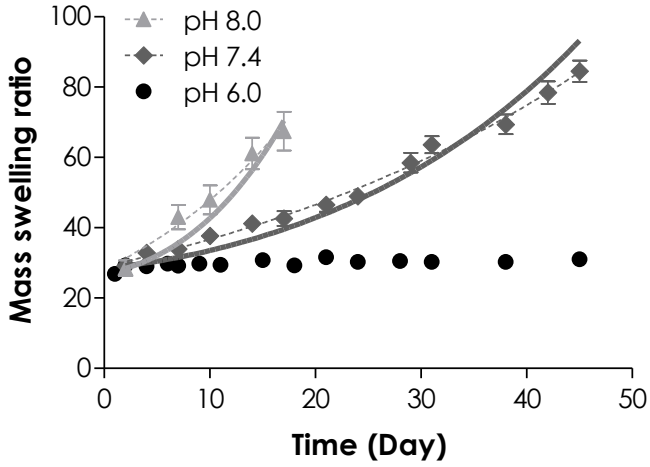

Figure 4.3 Effect of buffer pH on mass swelling ratio of 4 wt% PEG4NB-DTT hydrogels. Symbols represent experimental data while dashed curves represent exponential curve fitting to the experimental data. The apparent degradation rate constants (k_{hyd}) for gels degraded in pH 7.4 and pH 8.0 were 0.024 ± 0.001 and 0.057 ± 0.002 day^{-1}, respectively. Solid curves represent model predictions with best-fit kinetic rate constants: $k'_{pH\ 7.4} = 0.011\ day^{-1}$ and $k'_{pH\ 8.0} = 0.027\ day^{-1}$. No curve fitting or model prediction was made for gels degraded in pH 6.0 due to the stability of gels in acidic conditions.

Since the two basic pH conditions yielded significantly different degradation rates (Table 4.2), we were interested to know if gel degradation in different pH values assumed the same degradation mechanism. A previous study concerning the degradation of thiol-acrylate photopolymer networks revealed that, if the degradation follows the same ester hydrolysis mechanism at an elevated pH value (e.g., from pH 7.4 to pH 8.0), the two degradation profiles could be described using a pseudo-first order equation [26]:

$$[Ester] = [Ester]_0 e^{-k'[OH^-]t} \quad (4.1)$$

If the network degradation was purely due to ester bond hydrolysis without the influences from other environmental factors, the degradation could be described using the same ester hydrolysis rate constant (*k'*). Using this *k'*, two degradation curves (at pH 7.4 and pH 8.0) would overlap after adjusting the degradation time to account for the 4-fold increase in the OH^- ion concentrations between the two pH values [26]. Similarly, the factor of 4 could be incorporated into *k'* to reflect the accelerated degradation kinetics. Consequently, one would expect to obtain a 4-fold increase in the ratio of the apparent degradation rate constants (k_{hyd}) for hydrogels degraded in the two pH values. However, the exponential curve fitting performed in Figure 4.3 (k_{hyd} = 0.024 ± 0.001 and 0.057 ± 0.002 day^{-1} pH 7.4 and pH 8.0, respectively) yielded a k_{hyd} ratio of 2.4, rather than the ideal 4-fold increase (Table 4.2). This significantly lowered k_{hyd} ratio suggested that the degradation was not solely governed by simple ester bond hydrolysis and other factors could also play a role on the degradation rate of these thiol-ene hydrogels.

In addition to the experimental work, we also utilized a statistical-*co*-kinetic model to predict the hydrolytic degradation of thiol-ene hydrogels. Using this model (Equation 3.11), we chose a best-fit *k'* of 0.011 day^{-1} (R^2 = 0.96) and 0.027 day^{-1} (R^2 = 0.95) for the degradation of 4 wt% PEG4NB-DTT hydrogels in pH 7.4 and pH 8.0, respectively (Table 4.2). Note that these *k'* values were selected only to validate the model predictions at different degradation conditions, and by no means to suggest any 'ideality' in the crosslinked network since the gels at these conditions were not 'ideal' as discussed in the previous sections. As stated above, if the thiol-ene network degradation

was governed solely by ester bond hydrolysis, a k' of 0.044 day^{-1} (4-fold of $k'_{pH7.4}$ = 0.011 day^{-1}) could be used to predict gel degradation occurred at pH 8.0. However, the best-fit k' was 0.027 day^{-1} (R^2 = 0.95) for degradation occurred at pH 8.0, which only yielded a ratio of 2.5 (compared to $k'_{pH7.4}$ = 0.011 day^{-1}), and again was much slower than the theoretical 4-fold difference (Table 4.2). A potential explanation for this phenomenon is base-catalyzed oxidation of thioether bond forming between norbornene and thiol groups (Figure 4.3), which was likely promoted at higher pH values [55] and influenced the rate of ester hydrolysis. Another possible reason for the lower-than-predicted degradation rate at higher pH values was that the degradation process produced acidic by-products (Figure 4.3), which decreased acidity and retarded the degradation. Furthermore investigations, however, are required to elucidate the exact mechanisms.

Table 4.2 Hydrolytic degradation rate constants for PEG4NB-DTT hydrogel network. (N = 4)

[PEG4NB] (wt%)	pH	k_{hyd} (day^{-1})	R^2_{khyd}	Ratio of $k_{hyd,\ pH\ 8.0}/k_{hyd,\ pH\ 7.4}$	k' (day^{-1})	$R^2_{k'}$	Ratio of $k'_{pH\ 8.0}/k'_{pH\ 7.4}$
4	7.4	0.024 ± 0.001	0.98	2.4	0.011	0.96	2.5
	8.0	0.057 ± 0.002	0.98		0.027	0.98	
10	7.4	0.020 ± 0.001	0.98	2.5	0.009	0.95	2.3
	8.0	0.050 ± 0.001	0.99		0.021	0.96	

4.2.3 Effect of Macromer Concentration on Degradation of PEG4NB-DTT Hydrogels

We further evaluated the hydrolytic degradation of PEG4NB-DTT hydrogels with different macromer concentrations (4 and 10 wt%) in pH 7.4 (Figure 4.4A) and pH 8.0 (Figure 4.4B). We observed experimentally that hydrogels prepared from a precursor solution containing lower weight content of PEG4NB (e.g., 4 wt%) degraded at a slightly faster rate, regardless of pH values (Table 4.2). This study suggested that the effect of macromer concentration affected not only the initial network crosslinking (i.e., network

ideality), but also the rate of network hydrolytic degradation. Previously, Metters *et al.* successfully predicted the degradation of step-growth Michael-type addition hydrogels crosslinked by multi-arm PEG-acrylate and DTT. In their study, the degradation profiles were predicted using a single *k'*, indicating the hydrolysis of thioether-ester bonds forming between PEG-acrylate and DTT was not affected by factors other than simple hydrolysis (e.g., macromer concentration, crosslinking efficiency, etc.). In fact, previous models developed for predicting the hydrolysis of PEG hydrogels were based on the assumptions that the factors affecting hydrolysis could be 'lumped' into a pseudo-first order hydrolysis rate constant or *k'* [14-16, 22]. These factors include water or hydronium ion concentrations, temperature, pH values, etc. For highly swollen hydrogels (q > 10), these factors are often negligible and thus the degradation profiles of the hydrogels could be predicted using the same *k'* regardless of macromer composition or degree of network crosslinking (under constant temperature and pH value). While the degradation of thiol-ene hydrogels was mediated by ester bond hydrolysis, our data suggested that it was also affected by other environmental and/or structural factors (such as densities of cyclic olefin groups and thioether bonds at different macromer contents).

(A) (B)

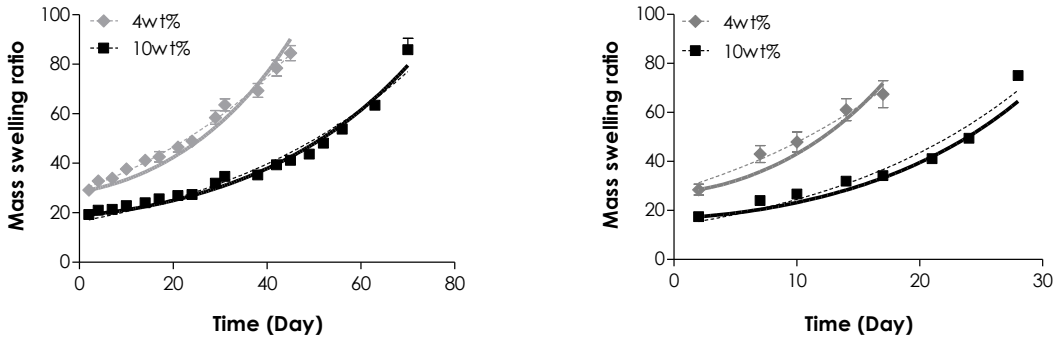

Figure 4.4 Hydrolytic degradation of PEG4NB-DTT hydrogels with different macromer concentrations in (A) pH 7.4 and (B) pH 8.0 PBS. Symbols represent experimental data, dashed curves represent exponential fit, and solid curves represent model prediction (See Table 4.2 for hydrolysis rate constants selected).

4.2.4 Effect of Initial Crosslinking Density on Degradation of PEG4NB-DTT Hydrogels

Results in Figure 4.4 revealed that the degradation rate of thiol-ene hydrogels could be affected by the degree of initial network crosslinking, a characteristic different from Michael-type addition hydrogels. In order to further validate this observation, we conducted additional studies using both theoretical and experimental approaches. We first predicted, using Equation 3.11, the degradation profiles of ideal thiol-ene hydrogels with different degrees of crosslinking by varying the stoichiometric ratios of thiol to ene moieties (i.e., $R_{[thiol]/[ene]}$ = 0.6, 0.8, and 1). This parametric manipulation yielded hydrogels with different initial crosslinking densities ($[A]_{0,\,ideal} = 5.78 \times 10^{-4}$, 7.71×10^{-4}, and 9.63×10^{-4} M for $R_{[thiol]/[ene]}$ = 0.6, 0.8, and 1, respectively). In these predictions, a fixed hydrolysis rate constant ($k' = 0.063$ day^{-1}) was selected based on a value reported for the degradation of step-growth Michael-type hydrogels [56]. As shown in Figure 4.5, the ideal initial mass swelling ratio at different degree of network crosslinking ($R_{[thiol]/[ene]}$ = 0.6, 0.8 and 1) varied only slightly between 9.6 and 11.9. Since the assumption in this prediction was that the rate of degradation is independent of the initial degree of network crosslinking, a single k' (0.063 day^{-1}) was used to predict the degradation profiles at various degrees of initial network crosslinking. Using this k', one can see that the three degradation profiles display slight variations.

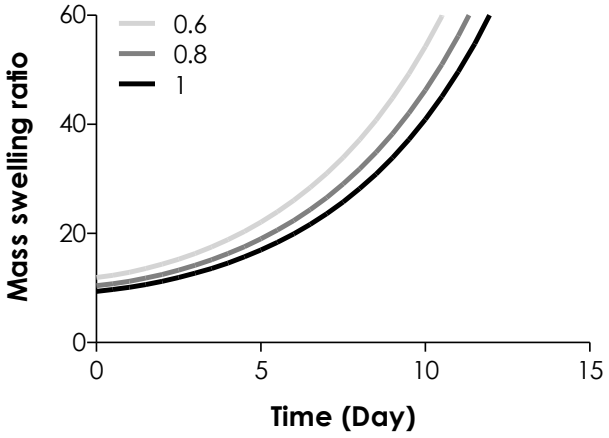

Figure 4.5 Model prediction of thiol-ene hydrogel degradation starting from different initial crosslinking ($R_{[thiol]/[ene]}$ = 0.6, 0.8 and 1; $k' = 0.063$ day^{-1}).

To validate the prediction shown in Figure 4.5, we designed thiol-ene hydrogels with different initial degree of crosslinking by altering the concentrations of crosslinker used (DTT, $R_{[thiol]/[ene]}$ = 0.6, 0.8 and 1) while keeping a constant PEG4NB macromer content (4 wt%) during gelation. As expected, decreasing initial network crosslinking (e.g., $R_{[thiol]/[ene]}$ = 0.6) resulted in a significant increase in initial hydrogel swelling (q = 69.2 ± 3.0) due to increased network non-ideality (Figure 4.6A). This phenomenon was similar to the results shown in Figure 4.2 where hydrogels prepared from lower PEG4NB weight contents had significantly higher initial swelling. When the difference in the initial degree of swelling was taking into account in model prediction, one would expect similar degradation trends as shown in Figure 4.5 where the profiles could be predicted using a single *k'*. Interestingly, our experimental results showed that thiol-ene network crosslinked with low $R_{[thiol]/[ene]}$ exhibited not only very high equilibrium swelling ratios, but also much faster degradation rates (Table 4.3). When the degradation profiles were fitted with Equation 3.11, the best-fit *k'* values were 0.035, 0.017, and 0.011 day^{-1} for $R_{[thiol]/[ene]}$ = 0.6, 0.8, and 1, respectively (Table 4.3). In another word, the degradation rate constants were accelerated (2- to 3-fold) as a function of network non-ideality. These results were different from previous reports for Michael-type hydrogels where a single *k'* could be used to describe the degradation occurred at different initial crosslinking densities. [22] The accelerated gel degradation was confirmed via rheometrical measurements where gels reached complete disintegration by day 21 and day 28 for $R_{[thiol]/[ene]}$ = 0.6 and 0.8, respectively (Figure 4.6B). While the mechanisms or factors affecting the hydrolytic degradation rate of thiol-ene hydrogels at different initial crosslinking densities are unknown, a general trend observed from our studies was that thiol-ene hydrogels with higher degree of crosslinking degraded at a slower rate than gels with lower degree of crosslinking.

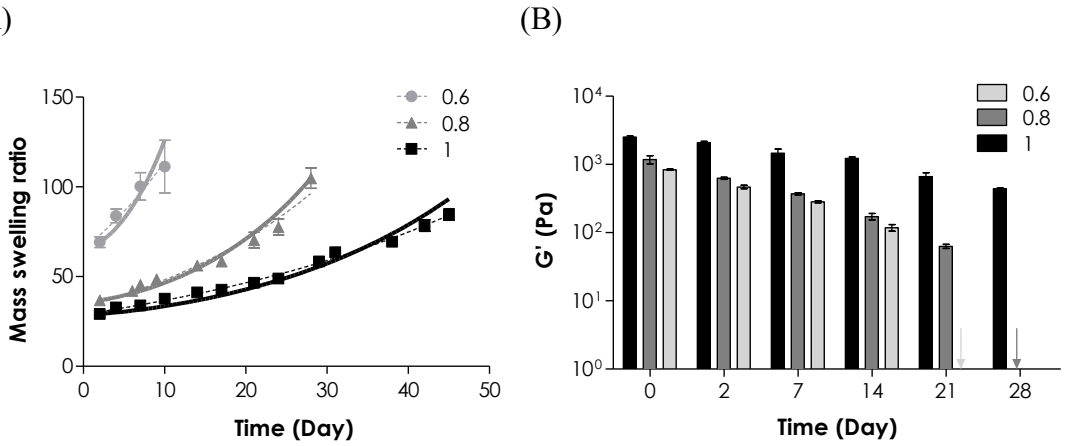

Figure 4.6 Effect of initial network crosslinking on PEG4NB-DTT hydrolytic degradation. (A) Mass swelling ratio and (B) elastic moduli of 4 wt% PEG4NB-DTT hydrogels with $R_{[thiol]/[ene]}$ = 0.6, 0.8, and 1. Symbols represent experimental data, dashed curves represent exponential fit, and solid curves represent model prediction (See Table 4.3 for degradation rate constants selected).

Table 4.3 Hydrolytic degradation rate constants for PEG4NB-DTT hydrogel network with different stoichiometric ratios. (N = 4)

$R_{[thiol]/[ene]}$	$[A]_{0,\ ideal}$ (M)	k_{hyd} (day^{-1})	R^2_{khyd}	k' (day^{-1})	$R^2_{k'}$
0.6	5.78×10^{-4}	0.073 ± 0.002	0.96	0.035	0.95
0.8	7.71×10^{-4}	0.035 ± 0.004	0.97	0.017	0.96
1	9.63×10^{-4}	0.024 ± 0.001	0.98	0.011	0.96

4.2.5 Effect of Crosslinker Sequence on Network Properties of PEG4NB-peptide Hydrogels

In previous sections, we have learned that there was a high inter-dependency between the degree of thiol-ene hydrogel network crosslinking and the subsequent degradation rates using DTT as a hydrogel crosslinker. Recent studies have shown that PEG hydrogels crosslinked by peptide crosslinkers are useful in creating biomimetic extracellular microenvironments [5, 21]. Here, we investigated the influence of peptide sequences on the crosslinking and degradation of step-growth thiol-ene hydrogels. As a model system to illustrate the importance of peptide sequences on thiol-ene hydrogel

degradation, we synthesized six simple peptide crosslinkers with amino acid variation: CGGGC, CGGYC, CGGLC, CGGKC, CGGDC and CDGDC. The molecular weights of these six peptide crosslinkers (MW_B) varied slightly between 394 to 511 Da (Table 4.4), which would only cause minimum influence in the chain length between adjacent crosslinks due to the relatively large PEG4NB macromolecules (MW_A = 20 kDa) used.

Table 4.4 Parameters for PEG4NB-peptide hydrogel network. (pH 7.4, N = 4)

Peptide Crosslinker	MW_B (Da)	Gel Point (sec)	k_{hyd} (day^{-1})	R^2_{khyd}	k' (day^{-1})	$R^2_{k'}$
CGGGC	394	5.3 ± 0.1	0.049 ± 0.001	0.98	0.026	0.96
CGGYC	501	4.5 ± 0.5	0.036 ± 0.004	0.99	0.018	0.98
CGGLC	451	4.3 ± 1.4	0.036 ± 0.002	0.99	0.017	0.98
CGGKC	466	20.3 ± 0.1	0.020 ± 0.015	0.62	N.A.	
CGGDC	453	2.9 ± 0.6	0.038 ± 0.001	0.94		
CDGDC	511	2.6 ± 1.2	0.027 ± 0.001	0.97		

Table 4.4 shows the biophysical properties of 4 wt% PEG4NB-peptide hydrogels crosslinked by peptide crosslinker with different sequences. These PEG4NB-peptide hydrogels all had rapid gel points (~4 to 5 seconds), which were consistent with our previous studies in thiol-ene hydrogels [3]. Similar to the degradation of PEG4NB-DTT gels shown in Figure 4.4 and 4.6, PEG-peptide hydrogel degradation rates were affected by the initial degree of network crosslinking. As shown in Figure 4.7, peptide sequences affected both initial crosslinking as well as subsequent hydrolytic degradation rate. At the same macromer weight content (4 wt%), the initial swelling ratios of PEG4NB-peptide hydrogels were significantly higher than that of PEG4NB-DTT hydrogels. As a result, these PEG4NB-peptide hydrogels exhibited faster hydrolytic degradation rates (Table 4.4). Interestingly, hydrogels crosslinked by CGGGC and CGGYC peptides had similar initial swelling (Figure 4.7A), but the degradation rate constant was significantly

lower for gels crosslinked by CGGYC (~26% lower in k_{hyd}; ~30% lower in k'. Table 4.4). Furthermore, hydrogels crosslinked by peptides containing aromatic (e.g., CGGYC) or hydrophobic (e.g., CGGLC) residues yielded slower degradation rates compared to gels crosslinked by simple CGGGC linker, potentially due to steric hindrance and hydrophobic effect of tyrosine and leucine residues that retarded degradation (Table 4.4). As expected, the swelling of these PEG4NB-peptide hydrogels was inversely correlated to the elastic moduli (Figure 4.7B). Hydrogels crosslinked by CGGGC peptide degraded completely in about 15 days (modulus dropped from ~1.0 kPa to ~0.1 kPa from day 0 to day 14), while gels crosslinked with CGGYC or CGGLC lasted at least 21 days until complete gel disintegration. In addition, we also evaluated the effect of charged amino acid on thiol-ene hydrogels crosslinking (Figure 4.7C). When a positively charged amino acid, lysine (K), was incorporated, the gelation was significantly hindered resulting in prolonged gel point (Table 4.4, ~20 seconds). Conversely, when a negatively charged aspartic acid (D) was incorporated in the 5-mer crosslinking peptide, the rate of gelation was about 7-folds faster than having positively charged lysine (Table 4.4, ~3 seconds). We believe that the presence of negatively charged amino acid assisted hydrogen deprotonation from the cysteine. To further prove this, two aspartic acids were incorporated in a 5-mer peptide. As predicted, slightly faster gelation rate, lower swelling ratio (Figure 4.7C) and higher elastic modulus (Figure 4.7D) were observed when these peptide crosslinkers containing two aspartic acids were used. Note that model prediction was not employed to predict the swelling ratio of hydrogels crosslinked by charged peptides due to the assumptions made by Flory-Rehner theory. This study revealed that the degradation of thiol-ene hydrogels could be easily tuned by altering identity of the peptide crosslinkers.

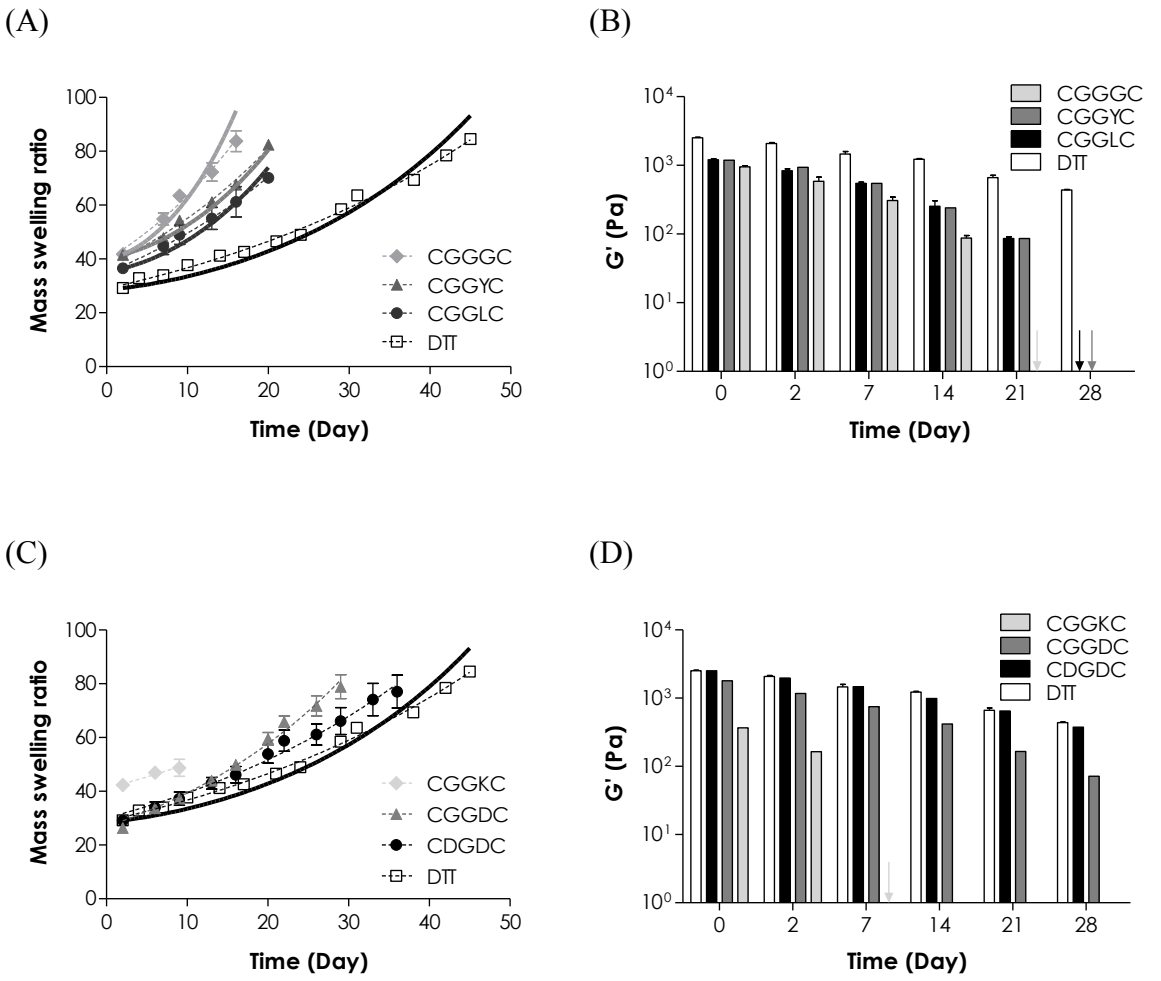

Figure 4.7 Effect of crosslinker peptide sequences on PEG4NB-peptide hydrogels degradation. (A) Mass swelling ratio and (B) elastic modulus of PEG4NB hydrogels crosslinked by CGGGC, CGGYC or CGGLC peptides. (C) Mass swelling ratio and (D) elastic modulus of PEG4NB hydrogels crosslinked by CGGKC, CGGDC or CDGDC peptides. PEG4NB-DTT hydrogels were used for comparison. Symbols represent experimental data, dashed curves represent exponential curve fits, and solid curves represent statistical-co-kinetics model fits to the experimental data. (4 wt% PEG4NB-peptide hydrogels, pH 7.4, N = 4)

4.2.6 Dual-mode Enzymatic and Hydrolytic Degradation of Thiol-ene Hydrogels

Many step-growth hydrogels have been prepared for protease-sensitive degradation by incorporating peptidyl substrates as hydrogel crosslinkers [3, 5, 8, 21, 57-61]. Here, we sought to combine enzymatic and hydrolytic degradation properties of thiol-ene hydrogels and create dual-mode degradable hydrogels without altering hydrogel molecular structure or hydrophilicity. By combining peptide crosslinkers with different protease sensitivities, we found that the degradation behaviors of thiol-ene hydrogels could be easily manipulated and changed from completely surface erosion to bulk degradation. Here, hydrogels were crosslinked by 4 wt% PEG4NB and stoichiometric ratio of non-cleavable CGGGC and/or chymotrypsin cleavable CGGY↓C peptides at various compositions (percent molar ratio of CGGYC:CGGGC = 100:0, 75:25, 50:50, 25:75 and 0:100, Figure 4.8). Note that the overall molar ratio of thiol to ene moieties was stoichiometric balanced for all conditions ($R_{[ene]/[thiol]} = 1$). When these gels were exposed to chymotrypsin solution, hydrogels contained high percentage of CGGYC crosslinker (100% to 75%) eroded rapidly by surface erosion, evidenced by linearly increasing mass loss profiles as time. These gels reached complete erosion at around 10 and 16 minutes for gels incorporated with 100% and 75% of CGGYC, respectively (Figure 4.8). Interestingly, when the total content of CGGYC peptide was decreased to 50% and 25%, chymotrypsin treatment led to increased gel mass (i.e., negative mass loss). These gels continued to swell and gained mass for the remaining course of study, indicating that protease treatment led to a 'loosened' gel structure and increased water uptake. The degradation mode was likely be transitioned from a surface erosion to a bulk degradation mechanism. On the other hand, chymotrypsin treatment had no effect on the swelling or mass loss of thiol-ene hydrogels crosslinked by non-chymotrypsin sensitive linker (CGGGC). These results suggested that by altering protease sensitivity of PEG4NB-peptide hydrogels through elegant selection of peptide crosslinkers, the mode of degradation profiles could also be manipulated and may be used to dynamically control growth factor delivery in the future.

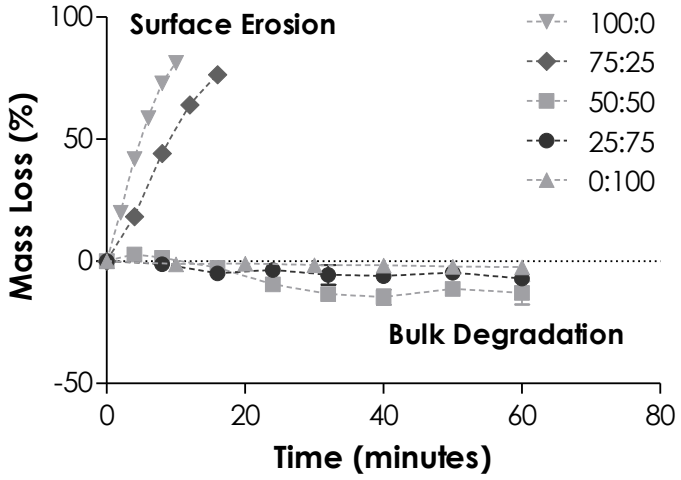

Figure 4.8 Effect of peptide crosslinkers on PEG4NB-peptide hydrogels erosion/degradation. PEG4NB hydrogels crosslinked by different percentage of chymotrypsin sensitive (CGGYC) and non-degradable (CGGGC) peptides. Figure legends indicate the percent molar ratio of CGGYC:CGGGC. (4 wt% PEG4NB-peptide hydrogels, pH 7.4, N = 4)

Additionally, 4 wt% PEG4NB-peptide hydrogels were prepared with chymotrypsin sensitive CGGYC and non-enzymatic degradable CDGDC at the percent molar ratio of CGGYC:CDGDC as 20:80. Here, CDGDC was selected due to its stability in hydrolytic degradation (Figure 4.7C). On specific days, these PEG4NB-peptide hydrogels were treated with chymotrypsin to selectively cleave CGGYC. This enzyme treatment intentionally cleaved the hydrogel network to increase the uptake of water. The resulting network was more susceptible to hydrolytic degradation compared to hydrogels that were not treated with chymotrypsin solution. In Figure 4.9, hydrogels that were not treated with chymotrypsin solution undergo steady degradation throughout 16 days. On the other hand, gels treated with chymotrypsin all reached complete disintegration by 16 days (swollen mass ~100 mg). For example, gels treated with chymotrypsin solution on day 2 had an accelerated rate of hydrolytic degradation and hydrogels degraded within 12 days. The resulted suggested potential applications in user-controlled therapeutic drug delivery and could be used to study biological phenomenon for controlling cell behavior.

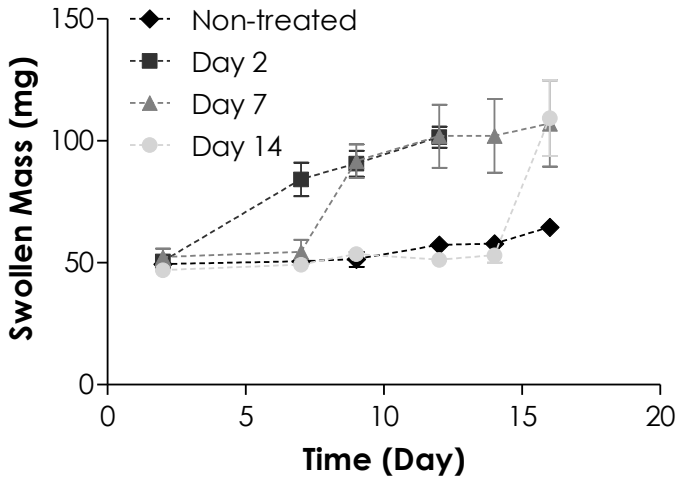

Figure 4.9 Effect of selective enzyme treatment on PEG4NB-peptide hydrogels erosion/degradation. PEG4NB hydrogels crosslinked by chymotrypsin sensitive (CGGYC) and non-degradable (CDGDC) peptides (percent molar ratio of CGGYC:CDGDC = 20:80). Figure legends indicate the specific day when gels were treated with chymotrypsin solution. (4 wt% PEG4NB-peptide hydrogels, pH 7.4, N = 4)

4.3 Visible Light-mediated Thiol-ene Hydrogelation Using Photoinitiator Eosin-Y

4.3.1 Gelation Kinetics: Step-growth Thiol-ene vs Chain-growth Photopolymerization

Thiol-norbornene photo-click hydrogels have increasingly been used in cell encapsulation studies [18, 20-22]. Prior reports on this new type of hydrogels, however, all used a cleavage type photoinitiator (I-2959 or LAP, Figure 1.2A and 1.2B) under 365 nm UV light exposure. Here, we demonstrate that thiol-norbornene gelation could be achieved using a visible light source (400 – 700 nm) with eosinY as the only photoinitiator (Figure 4.10). Upon visible light exposure, eosin-Y was excited to abstract hydrogen from thiol-containing crosslinkers, such as dithiothreitol (DTT), thus forming thiyl radicals. These radicals propagate through the norbornene moieties on multi-arm PEG macromers to form thioether bonds and carbonyl radicals. The termination of these carbonyl radicals is accomplished via abstracting hydrogen from other thiol-containing molecules [23].

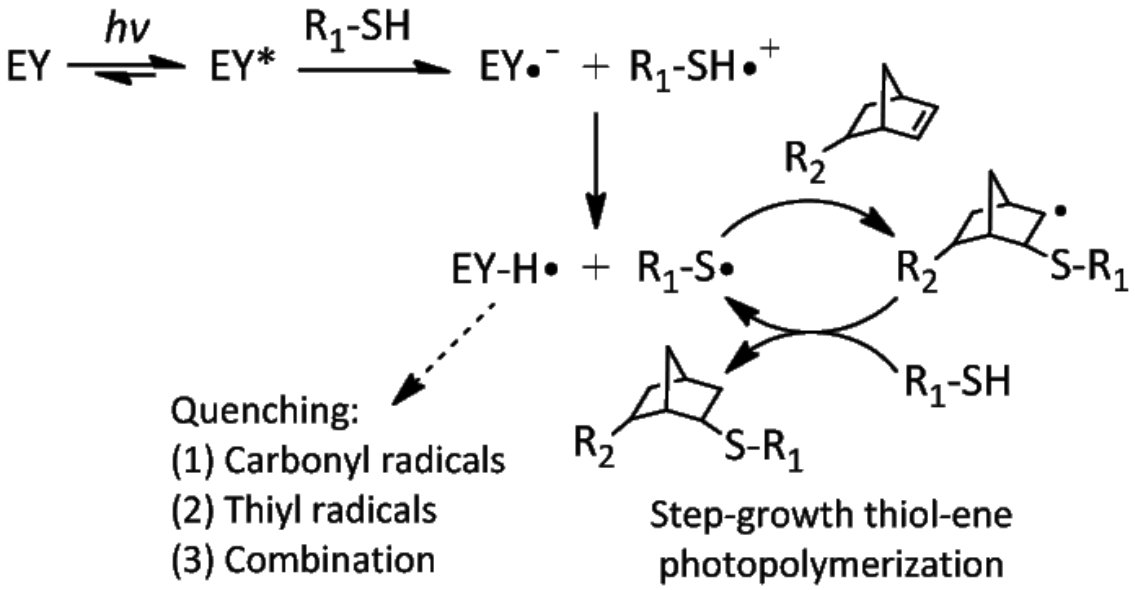

Figure 4.10 Initiation and polymerization mechanisms for visible light-mediated thiol-ene photopolymerization using eosin-Y (EY) as the sole photoinitiator which was excited by a visible light (400 to 700 nm) to initiate the photo-click reaction. The reactions result in gel cross-linking as R_1-SH and R_2-norbornene represents a bi- and tetra-functional cross-linker, respectively.

We first examined the gelation kinetics with *in situ* photo-rheometry in a light cure cell using 10 wt% $PEG4NB_{20kDa}$ (20 mM norbornene) and a stoichiometric-balanced thiol groups (from crosslinker DTT). 0.1 mM eosin-Y was added in the precursor solution as the photoinitiator. As shown in Figure 4.11A, this visible light-mediated step-growth thiol-ene reaction reached gel point rapidly (19 ± 2 seconds). The gel point was almost twice as fast as that in a conventional chain-growth PEGDA crosslinking reaction (37 ± 1 seconds) where equivalent macromer content (10 wt% $PEGDA_{10kDa}$ or 20 mM acrylate), a co-initiator (0.75 vol% TEOA) and a co-monomer (0.1 vol% NVP) were used (Figure 4.11B and Table 4.5). As described in the previous section, unlike chain-growth photopolymerizations of vinyl monomers (e.g., PEGDA), thiol-ene reactions are not oxygen inhibited [24], and hence resulted in a fast gelation even without using co-monomers.

(A) (B)

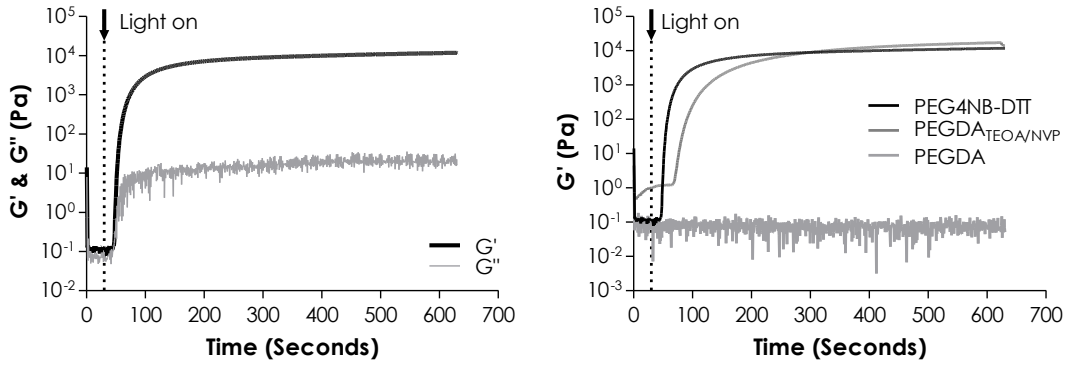

Figure 4.11 *In situ* photo-rheometry of: (A) Step-growth thiol-ene photo-gelation using PEG4NB and DTT. Eosin-Y was used as the only photoinitiator, which was excited by a visible light (400 to 700 nm) to initiate the photo-click reaction. (10 wt% or 5 mM PEG4NB-DTT, 0.1 mM eosin-Y, 70,000 Lux). (B) Chain-growth PEGDA hydrogels formed by visible light-mediated photopolymerizations (step-growth PEG4NB-DTT or chain-growth PEGDA hydrogels). Visible light (70,000 Lux) was turned on at 30 seconds. Gel compositions: 10 wt% PEGDA macromer and 0.1 mM eosin-Y for all gel formulations. 0.75 vol% TEOA and 0.1 vol% NVP added for chain-growth PEGDA gelation. (N = 3; error bars are omitted for clarity)

Table 4.5 Characteristics of hydrogels formed by visible light-mediated thiol-ene photopolymerization. (10 wt% PEG macromer and 0.1 mM of eosin-Y for all conditions. 0.75 vol% TEOA and 0.1 vol% NVP added for PEGDA gelation, N = 3)

Intensity (Lux)	Macromer system	Gel point (seconds)	G'$_{@\ 600\ sec}$ (kPa)
25,000*	PEG4NB-DTT	366 ± 19	0.15 ± 0.04
60,000 *	PEG4NB-DTT	114 ± 3	1.9 ± 0.5
70,000	PEG4NB-DTT	19 ± 2	12 ± 1.5
	PEGDA$_{TEOA/NVP}$	37 ± 1	17 ± 1.6

* At 600 seconds, this intensity did not yield complete gelation.

4.3.2 Effect of Light Intensity on Gel Properties

We also examined the gelation kinetics under different light intensities. Similar to other photopolymerization systems, significantly delayed gel points (19 ± 2 to 366 ± 19 seconds) and decreased final shear moduli (12 ± 1.5 to 0.15 ± 0.04 kPa) were obtained at lower light intensities (25,000 to 70,000 Lux, Figure 4.12 and Table 4.5). We found that this eosin-Y-only, visible light-mediated hydrogelation was unique to the thiol-norbornene system because gelation did not occur with PEG-tetra-acrylate alone unless co-initiator TEOA and co-monomer NVP were also added. Furthermore, we found that the co-monomer NVP, when added into the precursor solution, inhibited thiol-norbornene gelation. Further investigations are required to elucidate the underlying mechanisms.

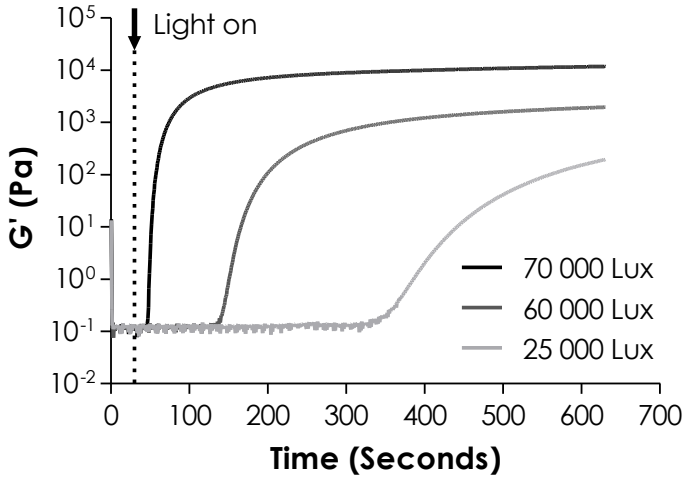

Figure 4.12 Effect of visible light intensity on the gelation kinetics of thiol-ene hydrogels (light was turned on at 30 seconds, N = 3). Error bars in figure were omitted for clarity.

4.3.3 Effect of Macromer Concentration on Gel Properties

We also evaluated the effect of macromer concentrations on network crosslinking using a gelation time of 4 minutes (G' higher than 95% of the final value, Figure 4.11A). As expected, there was an inverse correlation between macromer concentrations and gel points. Increasing macromer concentrations resulted in an increased in final gel moduli (Figure 4.13A) with accelerated gel points (Figure 4.13B). Furthermore, the gel fractions of thin hydrogels (thickness = 1 mm) were between 94% and 99% (Table 4.6), indicating

high gelation efficiency. Unlike chain growth PEGDA system where final gel moduli were affected by the necessary use of co-monomer NVP [15], the final moduli of visible light-mediated step-growth thiol-ene hydrogels were more readily controlled by macromer content in the precursor solution (Figure 4.13B). Eosin-Y is a red dye used in a common histological staining (i.e., Hematoxylin and eosin staining). Due to its intense red color, the thiol-ene gels formed with 0.1 mM eosin-Y appeared red-to-yellowish after gelation (Figure 4.13C). However, the color faded and the gels became transparent after swelling for 48 hours, suggesting that the eosin-Y may release into the buffer. As shown in Figure 4.13D, the equilibrium mass swelling ratios and shear moduli of these step-growth hydrogels exhibited high dependency on macromer concentration, indicating the existence of network non-ideality [25]. A similar trend in UV-mediated step-growth thiol-ene networks was observed in Figure 4.2 [23]. Furthermore, decreased network crosslinking efficiency was observed with thicker gel samples (3 mm), evidenced by decreased gel fractions and increased equilibrium swelling at lower macromer contents (Table 4.6). We believe this was due to higher light attenuation caused by red eosin-Y.

Table 4.6 Effect of gel thickness on gel fraction and equilibrium swelling ratio of hydrogels formed by visible light-mediated thiol-ene photopolymerization. (10 wt% PEG4NB-DTT, N = 3)

[PEG4NB] (wt%)	Gel fraction (%)		Swelling ratio	
	Gel thickness (mm)		Gel thickness (mm)	
	1	3	1	3
5	94.0 ± 2.1	80.6 ± 3.1	24.3 ± 1.9	32.7 ± 0.9
10	99.3 ± 1.2	90.5 ± 3.3	21.3 ± 0.1	23.3 ± 0.8
15	98.4 ± 0.6	93.2 ± 3.6	16.9 ± 0.8	18.5 ± 0.7
20	98.7 ± 0.6	95.8 ± 1.3	14.2 ± 0.1	17.4 ± 0.6

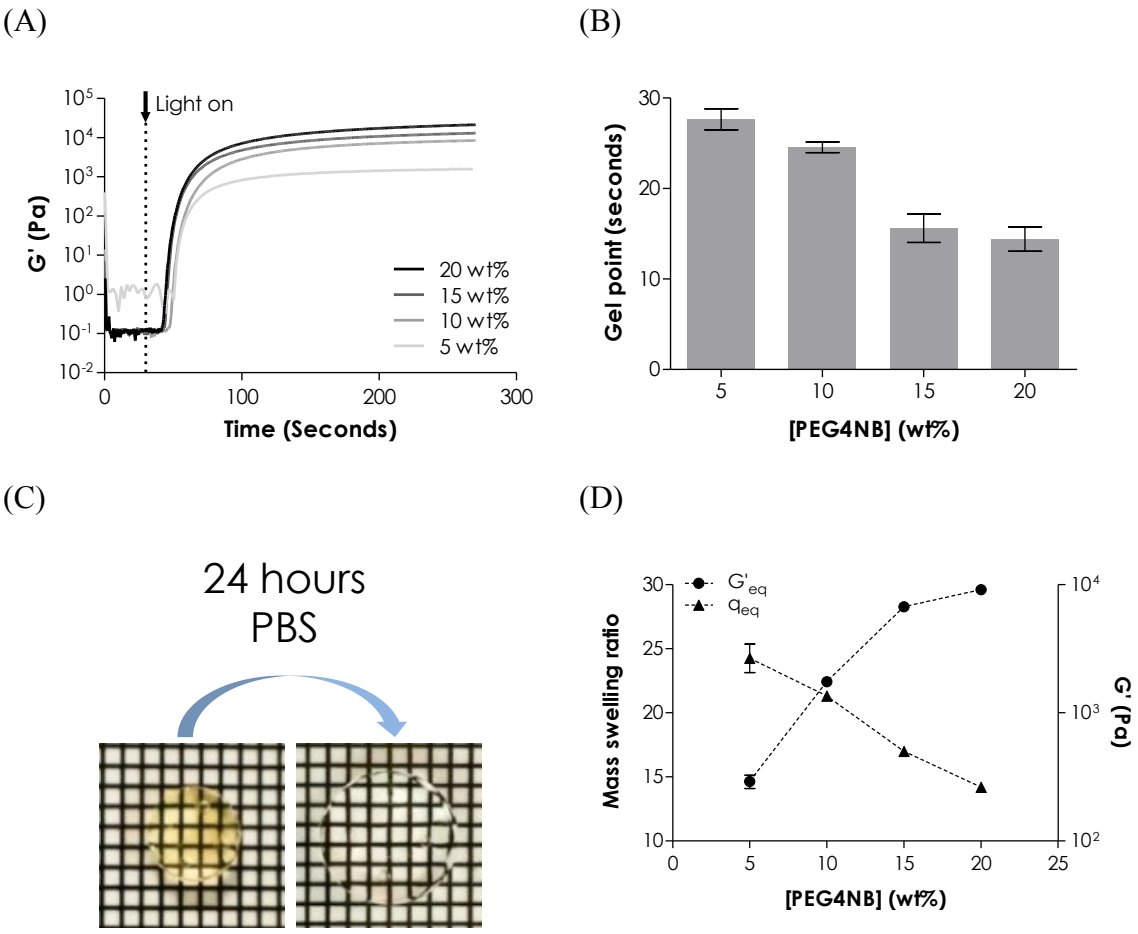

Figure 4.13 (A) Effect of macromer (PEG4NB) content on the gelation kinetics and (B) gel point. (C) Photographs of visible light-cured thiol-ene hydrogels (left) before and (right) after swelling for 24 hours (10 wt% PEG4NB with DTT as crosslinker, 0.1 mM eosin-Y as the initiator, length of a square grid = 1 mm). (D) Mass swelling ratio and elastic modulus of hydrogels at equilibrium swelling (N = 3). Error bars in (A) were omitted for clarity.

4.3.4 Effect of Eosin-Y Concentration on Gel Properties

We have shown that the cross-linking of step-growth thiol-norbornene hydrogels could be initiated by visible light exposure with eosin-Y as the only photoinitiator [62]. Here, we further explored this unique, simple, yet effective photopolymerization method for preparing step-growth hydrogels with multilayer structures. We first investigated the effect of initiator concentration on thiol-ene gelation kinetics. For thin samples such as those cured in the *in situ* photo-rheometry studies (100 μm, Figure 4.14A), increasing

eosin-Y concentration resulted in faster gelation rate as demonstrated by the rapid gel points shown in Figure 4.14B. For example, gelation using 2.0 mM eosin-Y reached gel point within 2 seconds or 10-fold faster than gelation with 0.1 mM eosin-Y (gel point ~24 seconds). The final elastic moduli of these thin gels, however, were ranging between ~6.4 kPa to ~9.1 kPa for different eosin-Y concentration used (0.1 to 2.0 mM, Figure 4.14A). As shown in Figure 4.10, eosin-Y was sensitized to an exited state upon visible light exposure [63]. The excited eosin-Y carbanion is capable of extracting hydrogen from proton-donating thiols, such as DTT or cysteine-bearing peptides/proteins, to generate thiyl radicals responsible for initiating thiol-ene photopolymerization and gelation [1]. The process repeats in a rapid step-growth manner to form a thiol-ene hydrogels [9]. Therefore, higher eosin-Y concentration leads to a higher initiation rate and faster gelation.

(A) (B)

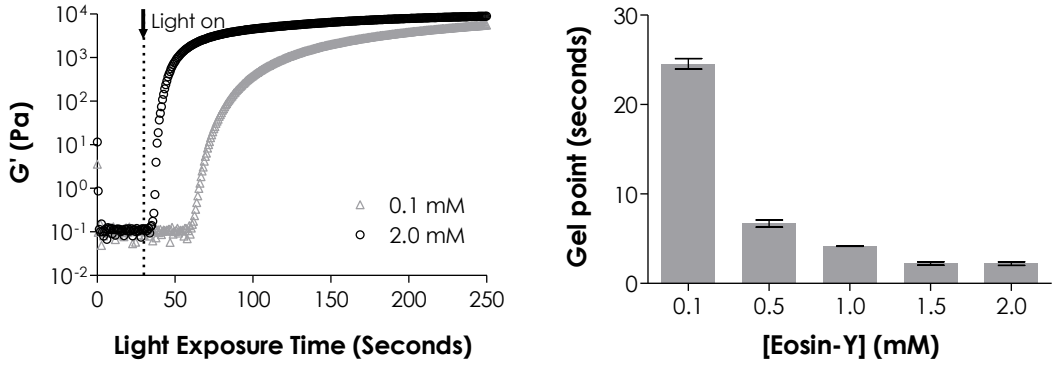

Figure 4.14 Effect of eosin-Y concentration on (A) gelation kinetics and (B) gel points of PEG4NB-DTT hydrogels formed by visible light-mediated thiol-ene photopolymerization. (PEG4NB: 10 wt%; N = 3)

While more initiators in the precursor solution accelerated initiation rate in thin hydrogel samples, higher eosin-Y concentration negatively affected network cross-linking efficiency in bulky hydrogels under the same gelling conditions (i.e., polymerization time and light intensity). This phenomenon was especially prominent for thicker gels. We fabricated thiol-ene hydrogels with two thicknesses (1 and 3 mm) using different eosin-Y concentrations (0.1 to 2.0 mM, polymerized for 4 minutes) and characterized gel fractions and equilibrium swelling ratios. As shown in Figure 4.15A, while thinner gels (e.g., 1 mm) had high gel fraction (> 95 %) regardless of eosin-Y concentrations, thicker gels (e.g., 3 mm) prepared with 2.0 mM eosin-Y had significantly lower gel fractions (72.5 ± 0.7 %) compared to gels prepared with 0.1 mM eosin-Y (90.5 ± 3.3 %). In general, gels with lower gel fractions reached higher equilibrium swelling ratios due to lower cross-linking efficiencies (Figure 4.15B) [9]. Interestingly, gels prepared with 1 mm thickness also exhibited higher swelling ratios at high eosin-Y concentrations (i.e., 1.5 and 2.0 mM), even though the dependency with eosin-Y concentration was less prominent compared to thicker gels. At higher eosin-Y concentrations, there is a higher tendency of eosin-Y quenching and termination that results in pendent polymer chains (Figure 4.10). While this type of network non-ideality did not cause reduction in gel fraction, it effectively decreases network cross-linking density that leads to higher gel swelling. For example, although all samples having a thickness of 1 mm have a similar gel fraction, the effects of light attenuation and eosin-Y quenching resulted in increased swelling ratio at high eosin-Y concentrations (e.g., 1.5 and 2.0 mM, Figure 4.15).

(A) (B)

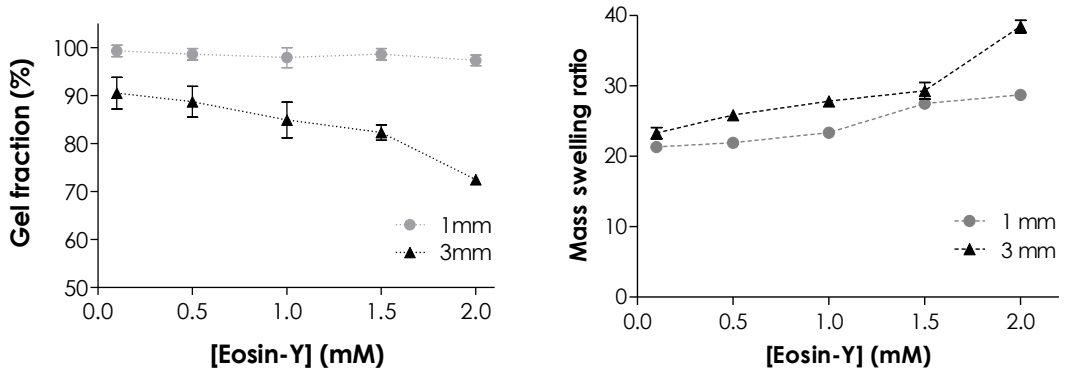

Figure 4.15 Effect of gel thickness and eosin-Y concentration on (A) gel fraction and (B) equilibrium swelling ratio of PEG4NB-DTT hydrogels formed by visible light-mediated thiol-ene photopolymerization for 4 minutes. (PEG4NB: 10 wt%; N = 3)

Comparing data presented in Figure 4.14 and Figure 4.15, it is clear that while eosin-Y serves as a visible light photoinitiator for thiol-ene reactions, it may also hinder network cross-linking, especially at a higher concentration or when it was used to form thicker gels. The lower gelation efficiency at a higher eosin-Y concentration was believed to be a result of a higher degree of light attenuation in thicker samples caused by the red eosin-Y. Light attenuation may result in slight network heterogeneity following cross-linking. However, due to the nature of orthogonal step-growth thiol-ene chemistry, these thiol-ene hydrogels will inherently be more homogeneous than all other chain-growth photopolymerized hydrogels. If desired, other parameters (e.g., light intensity and macromer concentrations) could be tuned to improve network cross-linking at higher eosin-Y concentration [62].

4.3.5 Sequestering of Eosin-Y in Thiol-ene Hydrogels

As shown in Figure 4.16A, gels cross-linked using higher eosin-Y concentrations appeared redder, even after extended (48 hours) incubation in PBS to leach out the residual dye. In addition, we found that a significant amount of eosin-Y became permanently sequestered in the gels in an eosin-Y concentration dependent manner

(Figure 4.16B). For example, after 48 hours incubation in PBS, roughly 26 nmol (or 25%) of eosin-Y retained in hydrogels fabricated using 2.0 mM eosin-Y. The sequestration of eosin-Y in these hydrogels was more noticeable in gels cross-linked with higher eosin-Y concentrations.

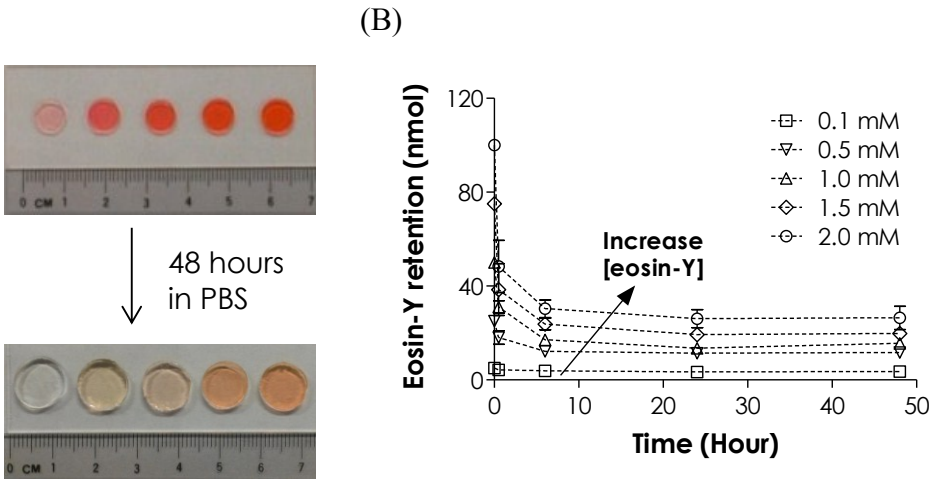

Figure 4.16 (A) Photographs of thiol-ene hydrogels formed by visible light-mediated, eosin-Y initiated thiol-ene photopolymerizations before (left) and after (right) swelling for 48 hours (eosin-Y concentration from left to right: 0.1, 0.5, 1.0, 1.5, 2.0 mM). (B) Effect of eosin-Y concentration on its retention in thiol-ene hydrogels. (PEG4NB: 10 wt%; N = 3)

The sequestration of eosin-Y in PEG hydrogels (mesh size: ~20 nm for 10 wt% PEG4NB-DTT hydrogels) was unexpected because it was unlikely for eosin-Y (MW ~692 Da) to be physically 'trapped' within the highly swollen and permeable gels. Based on the principles of radical polymerization, one potential explanation for the sequestration of eosin-Y is the quenching or termination reaction of protonated and radical-bearing eosin-Y (EY-H●) due to reactions with live carbonyl radicals on cross-linked PEG-norbornene or thiyl radicals on pendent DTT (Figure 4.10). A second possibility for the retention/sequestration of eosin-Y in the hydrogels was the existence of binding affinity between eosin-Y and these PEG hydrogels. To test the hypothesis of potential binding affinity between eosin-Y and thiol-ene hydrogel, UV/Vis absorbance

spectra of eosin-Y before and after visible light exposure were assessed in the presence of different relevant components (i.e., PEGdNB, DTT, or both) separately. The results shown in Figure 4.17A indicate that visible light exposure did not significantly affect the absorbance signature of eosin-Y (both maximum absorbance and peak wavelength). On the other hand, the inclusion of DTT not only decreased ~52 % of maximum absorbance, but also caused a slight shifting of eosin-Y peak wavelength from 517 nm to 505 nm (Figure 4.15B), suggesting the occurrence of photochemical reaction between DTT and eosin-Y. Interestingly, a shifting of peak wavelength from 516 nm to 522 nm was observed in the presence of PEGdNB with minimal change in maximum absorbance (Figure 4.17C). No spectrophotometric difference was found when PEGdNB was replaced with hydroxyl-terminated PEG (data not shown). Further, visible light exposure in the presence of eosin-Y, PEGdNB, and DTT (i.e., with thiol-ene reactions) resulted in a higher degree of reduction in eosin-Y maximum absorbance (~64 %), while the peak wavelength shifted from 522 nm to 510 nm (Figure 4.17D), a phenomenon similar to that shown in Figure 4.17B. The shifting in peak wavelength from 516 nm to 522 nm without chemical reaction suggests binding affinity between eosin-Y and PEG (potentially due to hydrogen bonds). On the other hand, visible light exposure in the presence of chemically reactive species (e.g., DTT and PEGdNB) caused a shifting of peak wavelength back to a lower value (i.e., 12 nm difference). This phenomenon implies a change in eosin-Y molecular structure, potentially due to reactions between excited eosin-Y and the reactive macromer species (e.g., adduct to PEG hydrogel network).

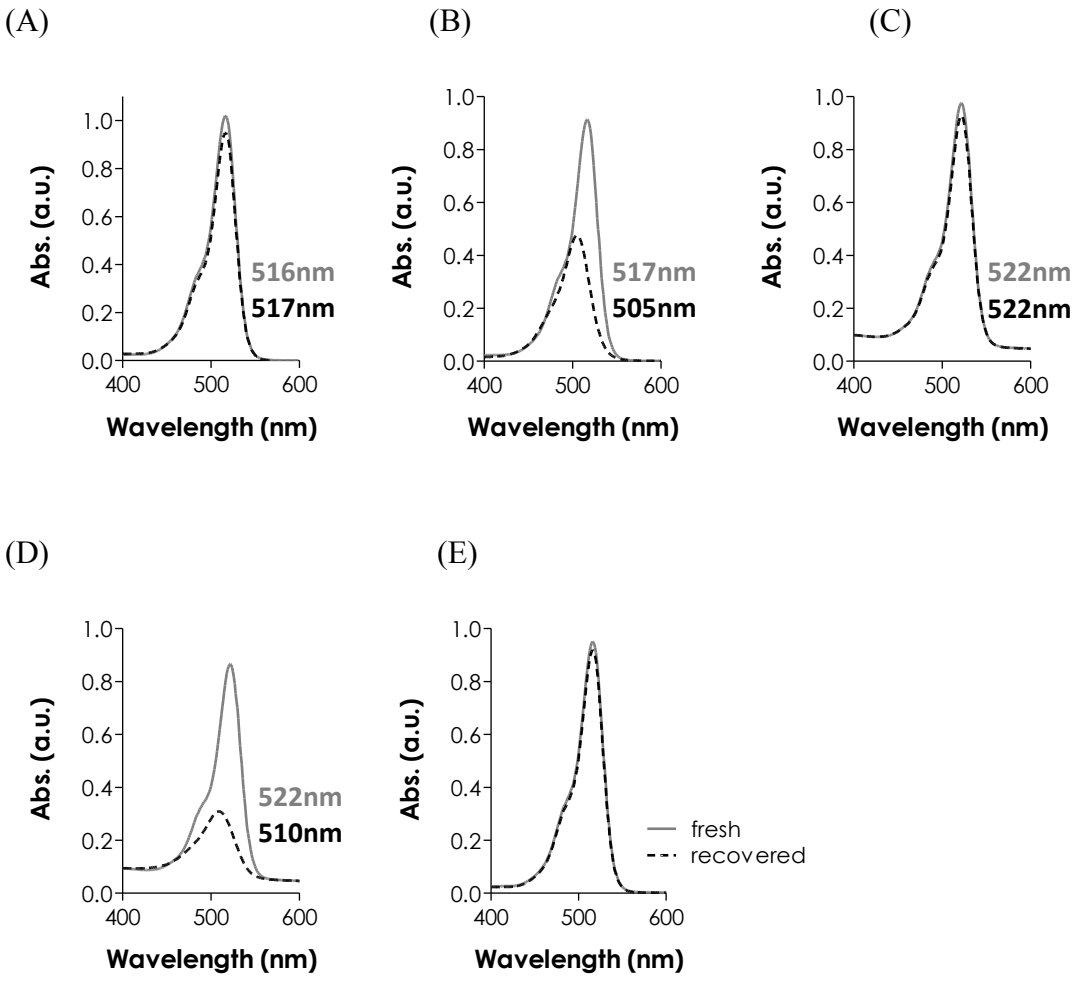

Figure 4.17 UV/Vis spectra of eosin-Y before (solid line) and after (dashed line) visible light exposure for 4 minutes in the presence of different components: (A) eosin-Y only; (B) eosin-Y and DTT; (C) eosin-Y and PEGdNB; (D) eosin-Y, PEGdNB, and DTT. Wavelengths indicated in each figure represent the peak absorbance before (top) and after (bottom) light exposure. (E) UV/Vis spectra of freshly prepared (solid line) and recovered (dashed line) eosin-Y. The wavelength of the peak absorbance for both samples was at 516 nm. Eosin-Y concentration in all measurements: 0.02 mM (N = 3).

4.3.6 Re-excitability of Eosin-Y to Form Thiol-ene Hydrogels

As described earlier, excess eosin-Y was released into the buffer solution during hydrogel swelling. From results shown in Figure 4.17, it is clear that eosin-Y, even after light exposure, still absorbs light in the visible light range. Since eosin-Y is not a cleavage type photoinitiator, we hypothesized that the excess eosin-Y could be used to initiate additional thiol-ene photo-click reactions. To demonstrate this feasibility, the spectrophotometric property of eosin-Y recovered from a pre-formed hydrogel was evaluated and compared to freshly prepared eosin-Y at an equivalent concentration (0.02 mM). The absorbance spectrum of the recovered eosin-Y overlaps with freshly prepared eosin-Y and still peaked at 516 nm (Figure 4.17E), suggesting that eosin-Y could be re-excited for sequential cross-linking reactions. It is important to note that in Figure 4.17B and Figure 4.17D, the measurements were conducted in the presence of reactive species while the samples used in Figure 4.17E were recovered eosin-Y from a cross-linked PEG gels. When recovered eosin-Y (at 0.1 mM) was used to initiate visible light-mediated thiol-ene gel cross-linking, the gel point was roughly 10 seconds slower compared to gelation using fresh eosin-Y (Figure 4.18). Furthermore, a significantly lower elastic modulus (~3.6 and ~6.4 kPa for gels prepared using recovered and fresh eosin-Y, respectively) after 240 seconds of light exposure (Figure 4.18) and a lower gel fraction was obtained (92 % and 99 % for 1 mm thick gels prepared with recovered and fresh eosin-Y, respectively). While the recovered eosin-Y does not have the same initiation capacity compared to freshly prepared eosin-Y, it is important to note that the eosin-Y concentration was kept low at 0.1 mM and a higher concentration may be used to compensate the slightly lower initiation capacity. Nonetheless, recovered eosin-Y retained the ability to re-initiate thiol-ene photopolymerization to fabricate hydrogels or conjugate biomolecules.

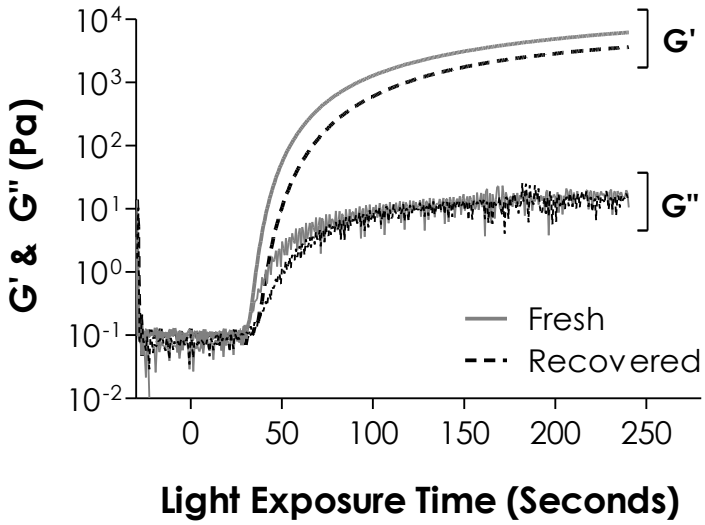

Figure 4.18 Evolution of elastic (G') and viscous (G") moduli during in situ gelation of PEG4NB-DTT using fresh or recovered eosin-Y at 0.1 mM as photoinitiator (PEG4NB: 10 wt%, N = 3). Error bars were neglected for clarity.

4.4 Cytocompatible and Multi-structural Thiol-ene Hydrogels Formed by Visible Light

4.4.1 Cytocompatibility of Thiol-ene Hydrogels Using Type II Photoinitiator

We evaluated the cytocompatibility of these visible light-mediated thiol-ene hydrogels using hMSCs (encapsulated at 5×10^6 cells/mL). Our results revealed that visible light-mediated thiol-ene hydrogels were highly cytocompatible for hMSCs following photoencapsulation (Figure 4.19A and 4.20, ~95 % initial viability determined by live/dead staining) and prolonged *in vitro* culture (Figure 4.19B). On the other hand, the viability of hMSCs encapsulated in conventional visible light-mediated chain-growth PEGDA hydrogels was relatively low and declined rapidly as time (Figure 4.19A and 4.19B). Although one may argue that the higher hMSC viability in thiol-ene hydrogels could be a result of hydrolytic degradation of PEG4NB hydrogels [23], our controlled experiments using hydrogels crosslinked by an amide-linked, non-degradable PEG4aNB macromer also supported higher degree of hMSC survival as compared to the chain-growth PEGDA hydrogel (Figure 4.19B). Interestingly, it was reported that visible light-

mediated chain-growth PEGDA gels supported survival of hMSCs [26]. In that particular study, however, the cells were encapsulated at an extremely high density (25×10^6 cells/mL), which might promote cell survival due to paracrine signaling. We also examined the cytocompatibility of hydrogels crosslinked by different concentrations of eosin-Y (0.1 and 1 mM) but did not find significant cellular damage even at high eosin-Y concentration (Figure 4.20).

(A)

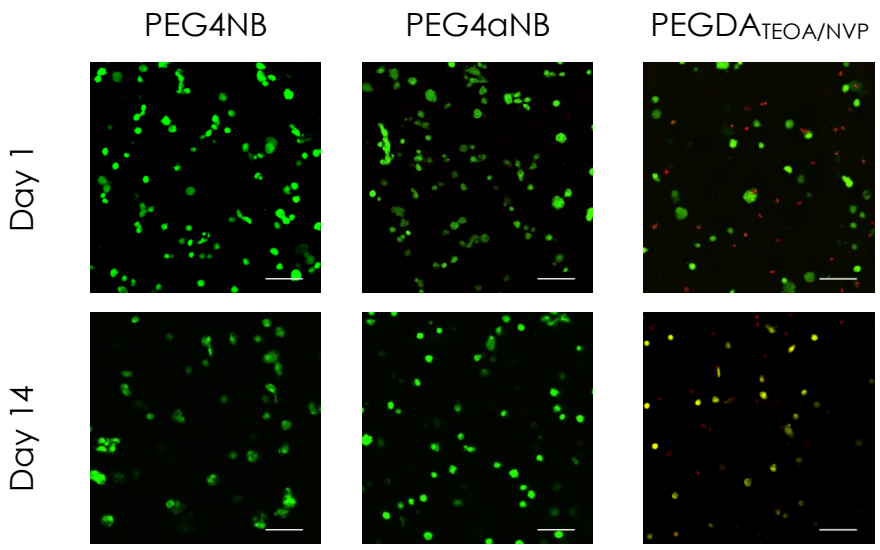

(B)

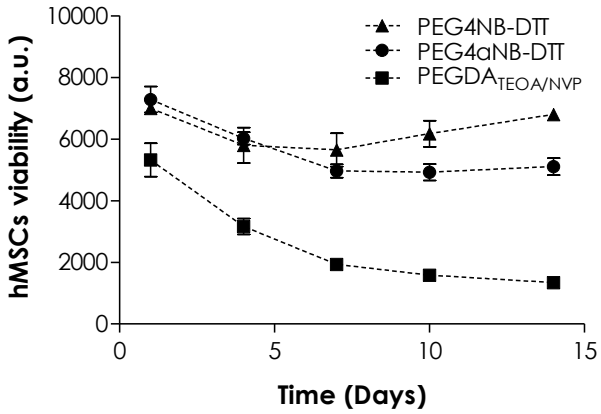

Figure 4.19 Cytocompatibility of visible light-mediated thiol-ene photopolymerizations. (A) Representative confocal z-stack images of hMSCs stained with Live/Dead staining kit on day 1 and 14. hMSCs were encapsulated (5×10^6 cells/mL) in step-growth degradable PEG4NB-DTT (left column) or non-degradable PEG4aNB-DTT (middle column) hydrogels, as well as chain-growth non-degradable PEGDA hydrogels (right column). All gel were fabricated with 10 wt% PEG macromer, 1 mM CRGDS, and 0.1 mM eosin-Y. In chain-growth PEGDA photopolymerization, TEOA (0.75 vol%) and of NVP (0.1 vol%) were added to facilitate gelation. (Scale: 100 μm). (B) hMSCs viability measured by Alamarblue® reagent (N = 3).

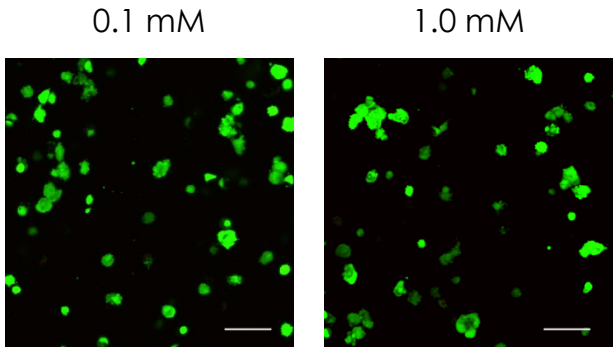

Figure 4.20 Confocal z-stack images of hMSCs stained with Live/Dead staining kit (day 1 post-encapsulation). hMSCs were encapsulated in 10 wt% PEG4NB-DTT hydrogels crosslinked using 0.1 or 1.0 mM eosin-Y (cell packing density: 5×10^6 cells/mL , scale: 100 μm).

An early and important application of visible light-mediated chain-growth PEGDA hydrogels was the formation of conformal coating for isolated islets [11]. We were interested in comparing the cytocompatibility of our visible light-initiated thiol-ene gels with the conventional PEGDA system by means of pancreatic β-cell encapsulation. We encapsulated radical sensitive MIN6 β-cells at 2×10^6 cells/mL in both systems and found that cell viability was significantly higher in the visible light-initiated thiol-ene gels compared to the PEGDA system (Top panel, Figure 4.21). Furthermore, MIN6 β-cells formed spherical aggregates only in the thiol-ene hydrogels but not in conventional PEGDA hydrogels (Bottom panel, Figure 4.21A). We have recently reported a similar result using UV-mediated thiol-ene photopolymerization [20]. We believe the significant cell death (for both hMSCs and MIN6) in the chain-growth PEGDA system was a collective result of high concentrations of radical species [27], formation of dense hydrophobic polyacrylate kinetic chains, and the potential cytotoxicity from TEOA and NVP.

(A)

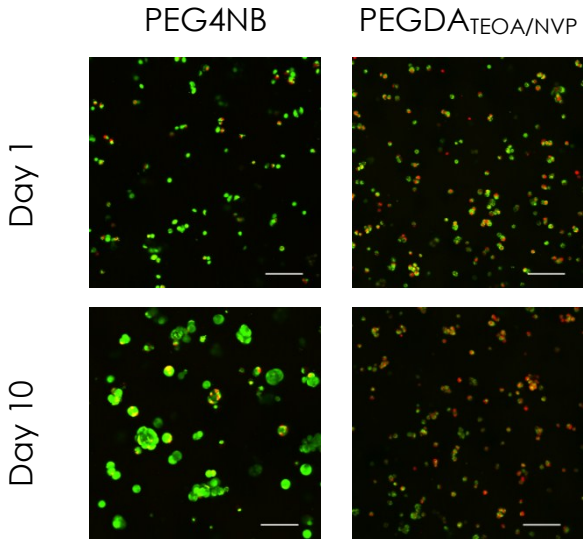

(B)

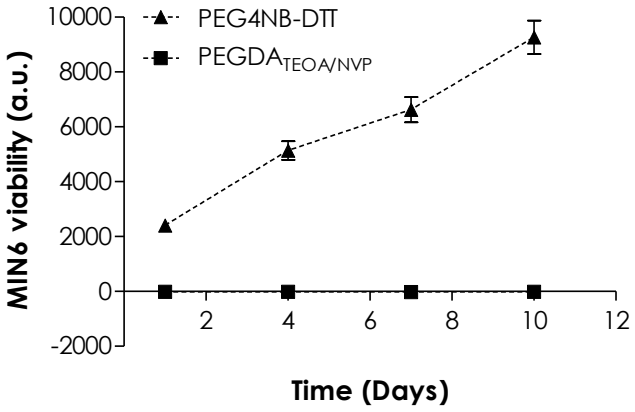

Figure 4.21 (A) Confocal z-stack images of MIN6 cells stained with Live/Dead staining kit. Cells were encapsulated in PEG4NB-DTT or PEGDA hydrogels using 0.1 mM eosin-Y (scale: 100 μm). (B) MIN6 viability quantified by Alamarblue® reagent. (10 wt% PEG hydrogels, cell packing density: 2×10^6 cells/mL, 0.75 vol% TEOA and 0.1 vol% of NVP were used in PEGDA hydrogels, N = 3, mean ± S.D.)

4.4.2 Multi-structure Thiol-ene Hydrogels

Proof-of-principle studies were conducted to explore the utility of the new interfacial thiol-ene gelation scheme on forming multilayer hydrogels. As shown in Figure 4.22A, we synthesized a three-layer hydrogel construct using sequential visible light-mediated thiol-ene photopolymerizations. To fabricate this simple multilayer hydrogel, we only added eosin-Y in the bottom layer. The formation of the middle and top layers was due to the diffusion of eosin-Y from the immediate adjacent layer. Although no additional initiator was added in the middle and top layers, the thickness of each layer after 10 minutes visible light exposure was similar (~2 mm). This was due to the use of a fixed pre-polymer solution volume (25 μL) in each layer and a three-fold higher light intensity (200,000 Lux) that resulted in complete gelation. Controlled experiments also showed that the formation of multilayer gels was not due to initiator-free polymerization as gelation did not occur (after 60 minutes light exposure) without the presence of eosin-Y. In addition, Figure 4.22B shows the formation of a thick gel coating (~ 5 mm diameter × 6 mm height cylinder) from a thin hydrogel disk (2 mm diameter × 1 mm height). This coating was formed without the inclusion of additional initiator in the coating macromer solution. More importantly, light attenuation was not a significant issue in forming this thick construct because there was no eosin-Y in the precursor solution and the gel cross-linking reaction was initiated from the surface of the core gel. The results of Figure 4.22A and 4.22B show that the formation of the multilayer construct was not solely due to eosin-Y diffusion but surface-mediated polymerization. In Figure 4.22, surface-mediated polymerization might have played a more significant role in allowing the growing of subsequent gel layers beyond the diffusional distant of eosin-Y. Due to the step-growth nature of the reactions, we believe that the properties in each layer will remain similar. However, from the view point of constructing biomimetic tissues with multilayer constructs, it is actually beneficial to have layer of gels with different properties. Future studies will focus on generation and characterization of multilayer gel structures with different material properties (e.g., crosslinking density, reaction kinetics, etc.).

While conventional visible light-mediated photopolymerization techniques could be used to fabricate multilayer hydrogels [44, 64, 65], additional initiating species and co-monomers are required to generate sufficient radicals for initiating cross-linking. Furthermore, prior visible light gelation systems were all based on chain-growth photopolymerization that has been shown detrimental to sensitive cells and growth factors [3, 46]. Chain-growth polymerized gels also have heterogeneous network structures [66], which may not be ideal for releasing therapeutically-relevant molecules. The unique visible light-mediated interfacial thiol-ene gel coating system is comparable to the glucose oxidase (GOx) mediated gel coating system reported by Bowman and colleagues [47-49]. The GOx-mediated gel coating system, however, uses multiple initiator components (i.e., GOx, glucose, and ferrous ion) to initiate polymerization reactions. Because the process produces highly cytotoxic hydrogen peroxide (H_2O_2), a second enzyme, catalase, has to be included in the macromer solution to prevent cellular damage. Another disadvantage of GOx-mediated polymer coating system is that GOx, being a bulky enzyme (R_h ~43 Å), is effectively trapped within the growing polymer layer. The presence of this additional component in the gel coating may cause unwanted complications. The interfacial thiol-ene gelation scheme presented here overcomes many disadvantages associated with other multilayer hydrogel systems and additional work is underway to exploit the utilities of this gel coating system in tissue engineering applications.

(A)

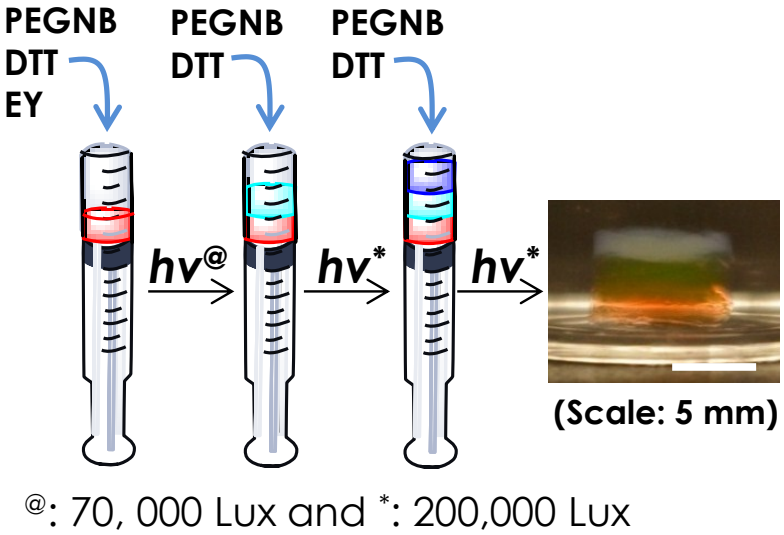

(B)

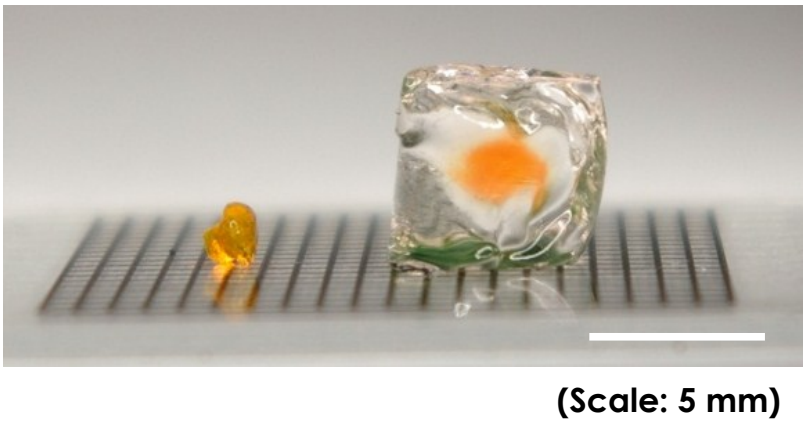

Figure 4.22 (A) Photograph of a three-layer thiol-ene hydrogel formed from sequential visible light-mediated thiol-ene photopolymerization. PEG4NB macromer concentration was 10 wt% in each layer. Eosin-Y concentration in the bottom layer was 2.0 mM. 5 wt% of blue microparticles was added in the top layer for visualization purpose. (B) Photograph of an example small gel disc (left, 2 mm diameter × 1 mm height) used to fabricate a thick gel coating (right, 6 mm diameter × 6 mm height). (Note: gel in the left curled up due to partial drying)

5. CONCLUSIONS AND RECOMMENDATIONS

In summary, we have shown that PEG hydrogels formed by step-growth thiol-ene photopolymerizations exhibited high degree of tunability in network crosslinking and degradation. In addition to the improved network properties compared to Michael-type hydrogels, we also found that thiol-ene hydrogels were hydrolytically degradable and the degradation was base-catalyzed and followed a bulk degradation mechanism. Through experimental and theoretical investigations, we found that the degradation of thiol-ene hydrogels was primarily governed by ester bond hydrolysis and was accelerated as network non-ideality increases. In addition, we were able to tune and predict the hydrolytic degradation behavior of thiol-ene hydrogels by manipulating the degree of network crosslinking and peptide crosslinker sequences. By altering thiol-ene hydrogel protease sensitivity, the mode of thiol-ene hydrogels degradation could be switched from surface erosion to bulk degradation. Furthermore, we have demonstrated an innovative approach for forming thiol-norbornene hydrogels by visible light-mediated, eosin-Y-initiated photo-click reactions. This gelation scheme preserves the rapid and efficient step-growth network crosslinking without the use of cytotoxic co-initiating components, thus ensuring high cytocompatibility for hMSCs and MIN6 β-cells. We have also developed a simple yet effective visible light-mediated interfacial thiol-ene photopolymerization scheme that can be used to create multilayer gel structures for biomedical applications. In addition to characterizing the effects of eosin-Y concentration on gel cross-linking efficiency, we also verified that part of the eosin-Y retained its ability to re-initiate thiol-ene photo-crosslinking. Utilizing this unique property, we have further designed step-growth hydrogels with multilayer structures and a wide range of thicknesses (from tens of microns to a few millimeters). No additional initiator is required in the preparation of hydrogel coating or multilayer gel, given that

sufficient eosin-Y is available from the core or adjacent hydrogel layers. This complete step-growth multilayer hydrogel system does not require and does not generate any cytotoxic components. Therefore, these multilayer gels may serve as a highly cytocompatible platform for creating complex multifunctional tissue substitutes.

This thesis work has demonstrated the three specific aims by exploring the degradability of thiol-ene hydrogels, developing an alternate approach to form cytocompatible thiol-ene hydrogels for cell encapsulation and demonstrating a light-dependent polymerization to form multilayer construct. Future investigations can focus on exploring the utility of using thiol-ene photo-click polymerization as a platform to study biological phenomenon. Future studies could focus on improving the statistical-*co*-kinetic model to predict degradability of thiol-ene hydrogels with various macromer or crosslinker functionalities. In addition, tissue engineering studies such as designing biomimetic microenvironements or stem cell niche could be conducted by exploiting the advantage of hydrogels degradability. The visible light-mediated thiol-ene photopolymerization could be employed in clinical-related studies. Lastly, further understanding on the generation and characterization of multilayer gel structures with different material properties (e.g., crosslinking density, reaction kinetics, etc.) could be useful for controlled multiple drugs or proteins delivery.

LIST OF REFERENCES

LIST OF REFERENCES

[1] B. D. Fairbanks, M. P. Schwartz, A. E. Halevi, C. R. Nuttelman, C. N. Bowman, and K. S. Anseth, "A versatile synthetic extracellular matrix mimic via thiol-norbornene photopolymerization," *Advanced Materials,* vol. 21, pp. 5005-5010, Dec 2009.

[2] C. E. Hoyle and C. N. Bowman, "Thiol-ene click chemistry," *Angewandte Chemie-International Edition,* vol. 49, pp. 1540-1573, 2010.

[3] C. C. Lin, A. Raza, and H. Shih, "PEG hydrogels formed by thiol-ene photo-click chemistry and their effect on the formation and recovery of insulin-secreting cell spheroids," *Biomaterials,* vol. 32, pp. 9685-9695, Dec 2011.

[4] B. D. Fairbanks, S. P. Singh, C. N. Bowman, and K. S. Anseth, "Photodegradable, Photoadaptable Hydrogels via Radical-Mediated Disulfide Fragmentation Reaction," *Macromolecules,* vol. 44, pp. 2444-2450, Apr 2011.

[5] S. B. Anderson, C. C. Lin, D. V. Kuntzler, and K. S. Anseth, "The performance of human mesenchymal stem cells encapsulated in cell-degradable polymer-peptide hydrogels," *Biomaterials,* vol. 32, pp. 3564-3574, May 2011.

[6] M. P. Schwartz, B. D. Fairbanks, R. E. Rogers, R. Rangarajan, M. H. Zaman, and K. S. Anseth, "A synthetic strategy for mimicking the extracellular matrix provides new insight about tumor cell migration," *Integrative Biology,* vol. 2, pp. 32-40, 2010.

[7] J. A. Benton, B. D. Fairbanks, and K. S. Anseth, "Characterization of valvular interstitial cell function in three dimensional matrix metalloproteinase degradable PEG hydrogels," *Biomaterials,* vol. 30, pp. 6593-603, Dec 2009.

[8] A. A. Aimetti, A. J. Machen, and K. S. Anseth, "Poly(ethylene glycol) hydrogels formed by thiol-ene photopolymerization for enzyme-responsive protein delivery," *Biomaterials,* vol. 30, pp. 6048-6054, Oct 2009.

[9] H. Shih and C. C. Lin, "Cross-linking and degradation of step-growth hydrogels formed by thiol-ene photoclick chemistry," *Biomacromolecules,* vol. 13, pp. 2003-2012, Jul 2012.

[10] K. S. Anseth, A. T. Metters, S. J. Bryant, P. J. Martens, J. H. Elisseeff, and C. N. Bowman, "In situ forming degradable networks and their application in tissue engineering and drug delivery," *Journal of Controlled Release,* vol. 78, pp. 199-209, Jan 2002.

[11] S. J. Bryant and K. S. Anseth, "Hydrogel properties influence ECM production by chondrocytes photoencapsulated in poly(ethylene glycol) hydrogels," *Journal of Biomedical Materials Research,* vol. 59, pp. 63-72, Jan 2002.

[12] N. A. Peppas, J. Z. Hilt, A. Khademhosseini, and R. Langer, "Hydrogels in biology and medicine: From molecular principles to bionanotechnology," *Advanced Materials,* vol. 18, pp. 1345-1360, Jun 2006.

[13] C. C. Lin and K. S. Anseth, "PEG hydrogels for the controlled release of biomolecules in regenerative medicine," *Pharmaceutical Research,* vol. 26, pp. 631-643, Mar 2009.

[14] A. T. Metters, K. S. Anseth, and C. N. Bowman, "Fundamental studies of a novel, biodegradable PEG-b-PLA hydrogel," *Polymer,* vol. 41, pp. 3993-4004, May 2000.

[15] A. T. Metters, C. N. Bowman, and K. S. Anseth, "A statistical kinetic model for the bulk degradation of PLA-b-PEG-b-PLA hydrogel networks," *Journal of Physical Chemistry B,* vol. 104, pp. 7043-7049, Aug 2000.

[16] A. T. Metters, K. S. Anseth, and C. N. Bowman, "A statistical kinetic model for the bulk degradation of PLA-b-PEG-b-PLA hydrogel networks: Incorporating network non-idealities," *Journal of Physical Chemistry B,* vol. 105, pp. 8069-8076, Aug 2001.

[17] A. S. Sawhney, C. P. Pathak, and J. A. Hubbell, "Bioerodible Hydrogels Based on Photopolymerized Poly(ethylene glycol)-co-Poly(alpha-hydroxy acid) Diacrylate Macromers," *Macromolecules,* vol. 26, pp. 581-587, Feb 1993.

[18] S. He, M. D. Timmer, M. J. Yaszemski, A. W. Yasko, P. S. Engel, and A. G. Mikos, "Synthesis of biodegradable poly(propylene fumarate) networks with poly(propylene fumarate)-diacrylate macromers as crosslinking agents and characterization of their degradation products," *Polymer,* vol. 42, pp. 1251-1260, Feb 2001.

[19] E. Cho, J. K. Kutty, K. Datar, J. S. Lee, N. R. Vyavahare, and K. Webb, "A novel synthetic route for the preparation of hydrolytically degradable synthetic hydrogels," *Journal of Biomedical Materials Research Part A,* vol. 90A, pp. 1073-1082, Sep 2009.

[20] D. L. Elbert, A. B. Pratt, M. P. Lutolf, S. Halstenberg, and J. A. Hubbell, "Protein delivery from materials formed by self-selective conjugate addition reactions," *Journal of Controlled Release,* vol. 76, pp. 11-25, Sep 2001.

[21] M. P. Lutolf, J. L. Lauer-Fields, H. G. Schmoekel, A. T. Metters, F. E. Weber, G. B. Fields, and J. A. Hubbell, "Synthetic matrix metalloproteinase-sensitive hydrogels for the conduction of tissue regeneration: Engineering cell-invasion characteristics," *Proceedings of the National Academy of Sciences of the United States of America,* vol. 100, pp. 5413-5418, Apr 2003.

[22] A. Metters and J. Hubbell, "Network formation and degradation behavior of hydrogels formed by Michael-type addition reactions," *Biomacromolecules,* vol. 6, pp. 290-301, Jan-Feb 2005.

[23] P. van de Wetering, A. T. Metters, R. G. Schoenmakers, and J. A. Hubbell, "Poly(ethylene glycol) hydrogels formed by conjugate addition with controllable swelling, degradation, and release of pharmaceutically active proteins," *Journal of Controlled Release,* vol. 102, pp. 619-627, Feb 2005.

[24] A. E. Rydholm, C. N. Bowman, and K. S. Anseth, "Degradable thiol-acrylate photopolymers: polymerization and degradation behavior of an in situ forming biomaterial," *Biomaterials,* vol. 26, pp. 4495-4506, Aug 2005.

[25] A. E. Rydholm, S. K. Reddy, K. S. Anseth, and C. N. Bowman, "Controlling network structure in degradable thiol-acrylate biomaterials to tune mass loss behavior," *Biomacromolecules,* vol. 7, pp. 2827-2836, Oct 2006.

[26] A. E. Rydholm, K. S. Anseth, and C. N. Bowman, "Effects of neighboring sulfides and pH on ester hydrolysis in thiol-acrylate photopolymers," *Acta Biomaterialia,* vol. 3, pp. 449-455, Jul 2007.

[27] A. E. Rydholm, S. K. Reddy, K. S. Anseth, and C. N. Bowman, "Development and characterization of degradable thiol-allyl ether photopolymers," *Polymer,* vol. 48, pp. 4589-4600, Jul 2007.

[28] S. P. Zustiak and J. B. Leach, "Hydrolytically Degradable Poly(Ethylene Glycol) Hydrogel Scaffolds with Tunable Degradation and Mechanical Properties," *Biomacromolecules,* vol. 11, pp. 1348-1357, May 2010.

[29] S. P. Zustiak and J. B. Leach, "Characterization of Protein Release From Hydrolytically Degradable Poly(Ethylene Glycol) Hydrogels," *Biotechnology and Bioengineering,* vol. 108, pp. 197-206, Jan 2011.

[30] S. Lin-Gibson, R. L. Jones, N. R. Washburn, and F. Horkay, "Structure-property relationships of photopolymerizable poly(ethylene glycol) dimethacrylate hydrogels," *Macromolecules,* vol. 38, pp. 2897-2902, Apr 2005.

[31] J. V. Karpiak, Y. Ner, and A. Almutairi, "Density gradient multilayer polymerization for creating complex tissue," *Advanced Materials,* vol. 24, pp. 1466-1470, Mar 2012.

[32] Z. S. Liu and P. Calvert, "Multilayer hydrogels as muscle-like actuators," *Advanced Materials,* vol. 12, pp. 288-291, Feb 2000.

[33] Y. J. An and J. A. Hubbell, "Intraarterial protein delivery via intimally-adherent bilayer hydrogels," *Journal of Controlled Release,* vol. 64, pp. 205-215, Feb 2000.

[34] A. A. Antipov, G. B. Sukhorukov, E. Donath, and H. Mohwald, "Sustained release properties of polyelectrolyte multilayer capsules," *Journal of Physical Chemistry B,* vol. 105, pp. 2281-2284, Mar 2001.

[35] J. T. Zhang, L. S. Chua, and D. M. Lynn, "Multilayered thin films that sustain the release of functional DNA under physiological conditions," *Langmuir,* vol. 20, pp. 8015-8021, Sep 2004.

[36] K. C. Wood, J. Q. Boedicker, D. M. Lynn, and P. T. Hammond, "Tunable drug release from hydrolytically degradable layer-by-layer thin films," *Langmuir,* vol. 21, pp. 1603-1609, Feb 2005.

[37] S. Mehrotra, D. Lynam, R. Maloney, K. M. Pawelec, M. H. Tuszynski, I. Lee, C. Chan, and J. Sakamoto, "Time controlled protein release from layer-by-layer assembled multilayer functionalized agarose hydrogels," *Advanced Functional Materials,* vol. 20, pp. 247-258, Jan 2010.

[38] X. Y. Chen, W. Wu, Z. Z. Guo, J. Y. Xin, and J. S. Li, "Controlled insulin release from glucose-sensitive self-assembled multilayer films based on 21-arm star polymer," *Biomaterials,* vol. 32, pp. 1759-1766, Feb 2011.

[39] G. M. Cruise, O. D. Hegre, F. V. Lamberti, S. R. Hager, R. Hill, D. S. Scharp, and J. A. Hubbell, "In vitro and in vivo performance of porcine islets encapsulated in interfacially photopolymerized poly(ethylene glycol) diacrylate membranes," *Cell Transplantation,* vol. 8, pp. 293-306, May-Jun 1999.

[40] P. S. Hume, C. N. Bowman, and K. S. Anseth, "Functionalized PEG hydrogels through reactive dip-coating for the formation of immunoactive barriers," *Biomaterials,* vol. 32, pp. 6204-6212, Sep 2011.

[41] X. Zhang, H. Chen, and H. Y. Zhang, "Layer-by-layer assembly: from conventional to unconventional methods," *Chemical Communications,* pp. 1395-1405, 2007.

[42] Z. Y. Tang, Y. Wang, P. Podsiadlo, and N. A. Kotov, "Biomedical applications of layer-by-layer assembly: From biomimetics to tissue engineering," *Advanced Materials,* vol. 18, pp. 3203-3224, Dec 2006.

[43] K. T. Nguyen and J. L. West, "Photopolymerizable hydrogels for tissue engineering applications," *Biomaterials,* vol. 23, pp. 4307-4314, Nov 2002.

[44] S. Kizilel, E. Sawardecker, F. Teymour, and V. H. Perez-Luna, "Sequential formation of covalently bonded hydrogel multilayers through surface initiated photopolymerization," *Biomaterials,* vol. 27, pp. 1209-1215, Mar 2006.

[45] M. P. Cuchiara, A. C. B. Allen, T. M. Chen, J. S. Miller, and J. L. West, "Multilayer microfluidic PEGDA hydrogels," *Biomaterials,* vol. 31, pp. 5491-5497, Jul 2010.

[46] J. D. McCall and K. S. Anseth, "Thiol-ene photopolymerizations provide a facile method to encapsulate proteins and maintain their bioactivity," *Biomacromolecules,* vol. 13, pp. 2410-2417, Aug 2012.

[47] L. M. Johnson, B. D. Fairbanks, K. S. Anseth, and C. N. Bowman, "Enzyme-mediated redox initiation for hydrogel generation and cellular encapsulation," *Biomacromolecules,* vol. 10, pp. 3114-3121, Nov 2009.

[48] L. M. Johnson, C. A. DeForest, A. Pendurti, K. S. Anseth, and C. N. Bowman, "Formation of three-dimensional hydrogel multilayers using enzyme-mediated redox chain initiation," *Acs Applied Materials & Interfaces,* vol. 2, pp. 1963-1972, Jul 2010.

[49] R. Shenoy and C. N. Bowman, "Kinetics of interfacial radical polymerization initiated by a glucose-oxidase mediated redox system," *Biomaterials,* vol. 33, pp. 6909-6914, Oct 2012.

[50] B. D. Fairbanks, M. P. Schwartz, C. N. Bowman, and K. S. Anseth, "Photoinitiated polymerization of PEG-diacrylate with lithium phenyl-2,4,6-trimethylbenzoylphosphinate: polymerization rate and cytocompatibility," *Biomaterials,* vol. 30, pp. 6702-7, Dec 2009.

[51] P. Flory, *Principles in Polymer Chemistry*. Ithaca, NY: Cornell University Press, 1953.

[52] K. S. Anseth, C. N. Bowman, and L. BrannonPeppas, "Mechanical properties of hydrogels and their experimental determination," *Biomaterials,* vol. 17, pp. 1647-1657, Sep 1996.

[53] A. M. Kloxin, J. A. Benton, and K. S. Anseth, "In situ elasticity modulation with dynamic substrates to direct cell phenotype," *Biomaterials,* vol. 31, pp. 1-8, Jan 2010.

[54] A. M. Kloxin, C. J. Kloxin, C. N. Bowman, and K. S. Anseth, "Mechanical Properties of Cellularly Responsive Hydrogels and Their Experimental Determination," *Advanced Materials,* vol. 22, pp. 3484-3494, Aug 2010.

[55] A. Napoli, M. Valentini, N. Tirelli, M. Muller, and J. A. Hubbell, "Oxidation-responsive polymeric vesicles," *Nature Materials,* vol. 3, pp. 183-189, Mar 2004.

[56] J. W. DuBose, C. Cutshall, and A. T. Metters, "Controlled release of tethered molecules via engineered hydrogel degradation: Model development and validation," *Journal of Biomedical Materials Research Part A,* vol. 74A, pp. 104-116, Jul 2005.

[57] T. P. Kraehenbuehl, L. S. Ferreira, P. Zammaretti, J. A. Hubbell, and R. Langer, "Cell-responsive hydrogel for encapsulation of vascular cells," *Biomaterials,* vol. 30, pp. 4318-4324, Sep 2009.

[58] T. P. Kraehenbuehl, P. Zammaretti, A. J. Van der Vlies, R. G. Schoenmakers, M. P. Lutolf, M. E. Jaconi, and J. A. Hubbell, "Three-dimensional extracellular matrix-directed cardioprogenitor differentiation: Systematic modulation of a synthetic cell-responsive PEG-hydrogel," *Biomaterials,* vol. 29, pp. 2757-2766, Jun 2008.

[59] J. S. Miller, C. J. Shen, W. R. Legant, J. D. Baranski, B. L. Blakely, and C. S. Chen, "Bioactive hydrogels made from step-growth derived PEG-peptide macromers," *Biomaterials,* vol. 31, pp. 3736-3743, May 2010.

[60] J. Patterson and J. A. Hubbell, "Enhanced proteolytic degradation of molecularly engineered PEG hydrogels in response to MMP-1 and MMP-2," *Biomaterials,* vol. 31, pp. 7836-7845, Oct 2010.

[61] M. V. Tsurkan, K. Chwalek, K. R. Levental, U. Freudenberg, and C. Werner, "Modular StarPEG-Heparin Gels with Bifunctional Peptide Linkers," *Macromolecular Rapid Communications,* vol. 31, pp. 1529-1533, Sep 2010.

[62] H. Shih and C. C. Lin, "Visible light-mediated thiol-ene hydrogelation using eosin-Y as the only photoinitiator," *Macromolecular Rapid Communications,* vol. (In press), p. DOI: 10.1002/marc.201200605 2012.

[63] C. Grotzinger, D. Burget, P. Jacques, and J. P. Fouassier, "Visible light induced photopolymerization: speeding up the rate of polymerization by using co-initiators in dye/amine photoinitiating systems," *Polymer,* vol. 44, pp. 3671-3677, Jun 2003.

[64] G. Papavasiliou, P. Songprawat, V. Perez-Luna, E. Hammes, M. Morris, Y. C. Chiu, and E. Brey, "Three-dimensional patterning of poly(ethylene glycol) hydrogels through surface-initiated photopolymerization," *Tissue Engineering Part C-Methods,* vol. 14, pp. 129-140, Jun 2008.

[65] S. Kizilel, V. H. Perez-Luna, and F. Teymour, "Photopolymerization of poly(ethylene glycol) diacrylate on eosin-functionalized surfaces," *Langmuir,* vol. 20, pp. 8652-8658, Sep 2004.

[66] G. M. Cruise, O. D. Hegre, D. S. Scharp, and J. A. Hubbell, "A sensitivity study of the key parameters in the interfacial photopolymerization of poly(ethylene glycol) diacrylate upon porcine islets," *Biotechnology and Bioengineering,* vol. 57, pp. 655-665, Mar 1998.

APPENDICES

Appendix A

H^1NMR spectrum for PEG4NB (20kDa)

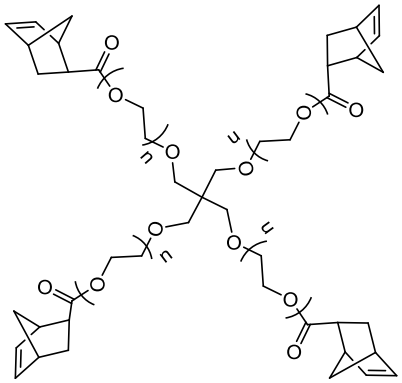

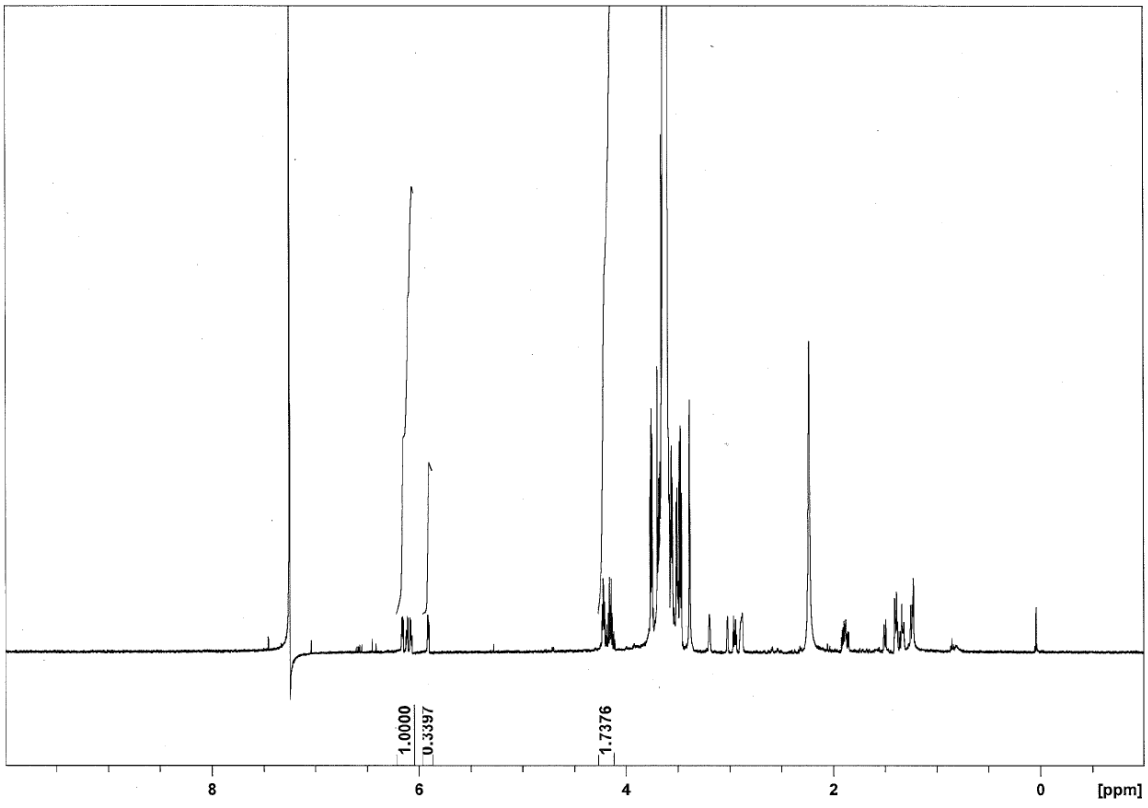

Appendix B

H^1NMR spectrum for PEG4aNB (20kDa)

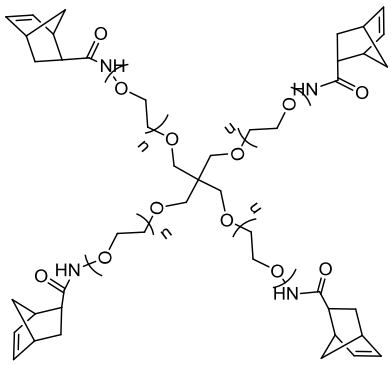

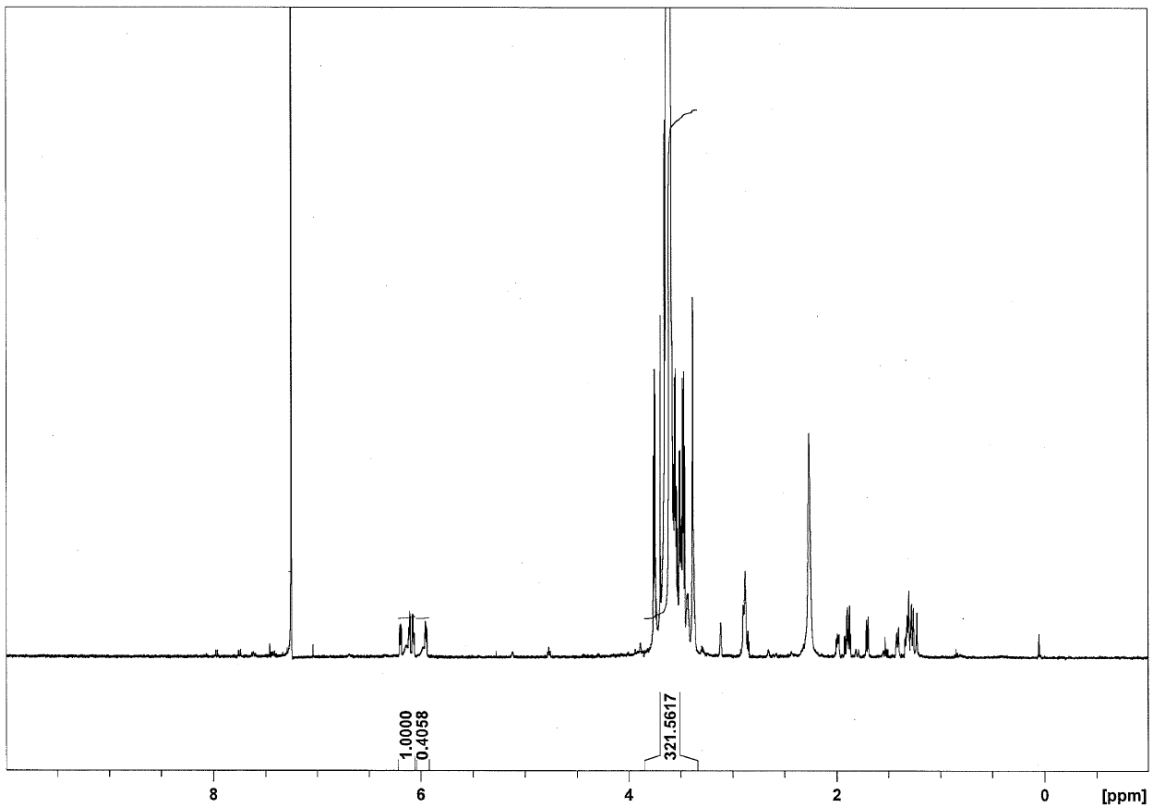

Appendix C

H^1NMR spectrum for PEG4A (20kDa)

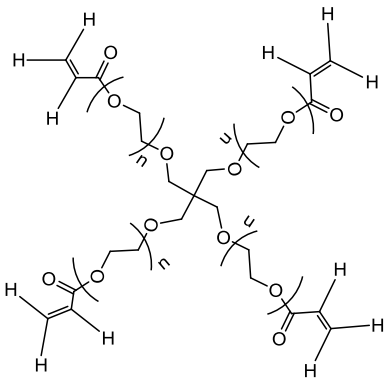

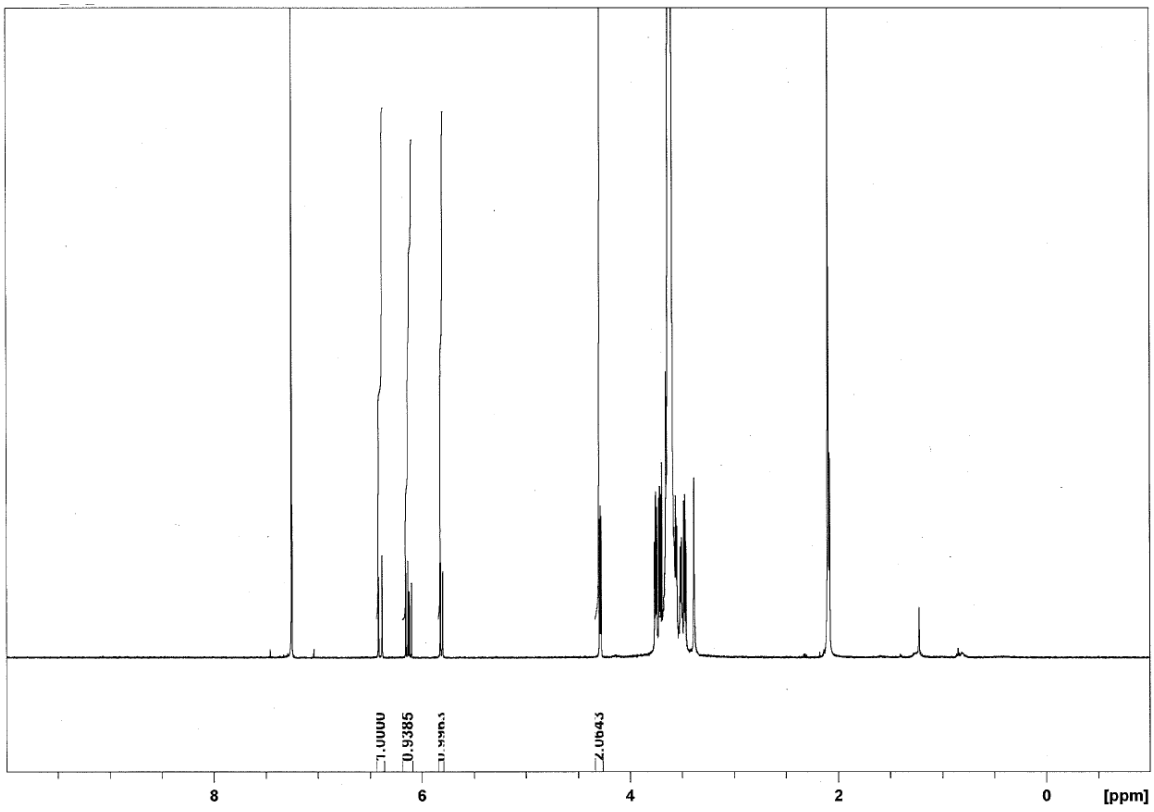

Appendix D

H^1NMR spectrum for LAP